Research Department

Technical Report No. 71

Results with a coupled wind wave model

Peter A E M Janssen[1]

BCRS Project 4.1/TO-06

[1] *KNMI, de Bilt, The Netherlands and ECMWF*

February 1994

ABSTRACT

Much of the work presented in this report is based on some ideas of two-way interaction of wind and waves developed by the author in the beginning of the 1980's. It took him 5 years to realise that these ideas could provide a reasonable estimate of the momentum transfer from air to the ocean and that there is a significant dependence of the surface stress on the sea state.

Because of the sea state dependence of momentum transfer it seemed plausible that a consistent momentum balance over the oceans could only be obtained by coupling an atmospheric model to a wave prediction model. Together with Liana Zambresky, Heinz Günther and Piero Lionello we worked out the consequences of two way interaction for wave prediction. As a result, Cy4 of the WAM model emerged, which since September 1991 is the operational wave prediction model at ECMWF. Here, I report work done together with Pedro Viterbo and Anton Beljaars on the consequences of two-way interaction for the atmospheric circulation.

The sea state dependence of momentum transfer has also consequences for scatterometry. The backscatter, namely, depends on the surface stress, and if one would like to infer information on the wind field then knowledge of the sea state dependent drag coefficient is required. It seems therefore natural to interpret the radar backscatter in the context of coupled wind-wave model. Here, I report on work done together with Hendrik Wallbrink and Han Janssen on the validation of the VIERS scatterometer against ERS-1 data. Also, some initial ideas on the sea state dependence of the radar backscatter by Peter Woiceshyn and myself are presented.

The overall impression of the work presented in this report is that it is worthwhile to develop further a coupled ocean-wave atmospheric model, because it seems beneficial for scatterometry and weather prediction in the medium range. The sea state dependent surface stress has a significant impact on the climate of the atmosphere. Furthermore, when forcing Dave Anderson's ocean circulation model with these surface stresses a considerable impact on the climate of the ocean is found. Anticipating the development of one model for our geophysical system, i.e. a coupled ocean-atmosphere model where the wave model provides the necessary interface between ocean and atmosphere, the wave dependent surface stress may induce therefore significant changes in the temperature distribution of the ocean. In its turn this may affect the climate of the atmosphere as well.

CONTENTS page

1. INTRODUCTION

There is increasing interest in the simulation of the earth's climate by means of coupled ocean-atmosphere models. First attempts towards direct coupling reveal, however, basic shortcomings in our knowledge of clouds and air-sea fluxes. The lack of knowledge of air-sea interaction is nicely illustrated by *Cubasch* (1989) where coupling of an atmospheric model (European Centre for Medium-Range Weather Forecasts (ECMWF) model with spectral resolution of T21 and 16 levels) with the ocean model of *Maier-Rainer et al* (1982) showed a definite trend in the mean atmospheric temperature. On the other hand, application of the flux correction method of *Sausen et al* (1988) removes this drift in the climate.

Although there is no doubt that by retuning cloud parametrization schemes the climate drift may be removed as well, it is believed that there is sufficient uncertainty in our knowledge of air-sea fluxes to warrant a more systematic investigation in this matter. To this end the Joint Scientific Committee of the World Climate Research Program (WCRP) and the Committee on Climate Changes and the Ocean (CCCO) have set up a working group on air-sea fluxes. Within this group consensus has been achieved about the most promising way to obtain a reliable data base of fluxes of momentum, heat and moisture at the air-sea interface. This is to perform an analysis using model surface fields of a sophisticated atmosphere model (eg the ECMWF model plus the third generation WAM model) with the wealth of wind and wave data from the next generation of satellites (such as ERS-1, ERS-2, ...).

Much progress into the understanding of the physics of wind-wave interaction has been achieved recently (*Donelan*, 1982), *Janssen* (1982), *Janssen* (1989a), *Janssen et al* (1989b), *Janssen* (1991), *Chalikov and Makin* (1991), *Maat et al* (1991), *Smith et al* 1992). All these studies suggest that the momentum flux depends on the sea state and therefore an optimal estimation of momentum transfer at the air-sea interface requires the development of a coupled ocean-wave, atmosphere model.

The new generation of satellites is able to observe the significant wave height (by means of the Radar Altimeter) and the wind vector (by means of the Scatterometer). The measurement theory of the Scatterometer is, however, still under development. From previous work (see eg BCRS report on VIERS-1 phase 3) it has become clear that the radar backscatter not only depends on wind speed and direction but also on the stability of the atmospheric boundary layer, the state of the long waves, the presence of slicks, etc. This suggests that the most optimal interpretation of the backscatter signal may be achieved in the context of a coupled ocean-wave, atmosphere model which provides information on sea state and atmospheric stability. It is therefore the intention to further develop and validate the scatterometer algorithm obtained during VIERS-1 using scatterometer return signals from ERS-1 and analysed fields from the ECMWF model.

As soon as a reliable scatterometer algorithm is available and as soon as a good coupled wind-wave model has been implemented, we can start with the development of a coupled wind-wave data assimilation system which respects the dependence of stress and scatterometer algorithm on the sea state thereby producing the most optimal analysis of momentum, heat and moisture flux.

Based on the above discussion, it was considered worthwhile to study the following elements:

- Testing of VIERS scatterometer algorithm using ERS-1 data set
- Implementation of a coupled wind-wave model
- Validation of coupled wind-wave model
- Development of coupled wind-wave data assimilation scheme
- Testing of data assimilation scheme
- Show feasibility of a reliable flux data base for climate purposes.

The present report describes the status of the work up to June 1993 and will discuss the first three items, namely testing of the scatterometer algorithm and the implementation and validation of a coupled wind-wave model.

2. TESTING OF VIERS-1 SCATTEROMETER ALGORITHM USING ECMWF WIND FIELDS AND ERS-1 BACKSCATTER

Traditionally, the operational retrieval algorithms for scatterometer relating the radar backscatter measurements to surface wind vectors have been empirical. The assumption that the backscatter only depends on the local wind field may be questioned, however, since the backscatter reflects in some way the state of the high-frequency wind waves. The spectrum of gravity-capillary waves generated by wind not only depends on the local wind, but is determined by a number of physical processes, namely wind input, nonlinear three and four wave interactions, viscous dissipation and dissipation due to slicks (cf VIERS-1 report (1993)). Thus, for high winds when the waves are sufficiently steep, nonlinear processes may be dominant so that the state of the gravity-capillary waves is mainly determined by the longer gravity waves. In that event, the radar backscatter is likely to depend on the history of the wind field and not on the local wind field. On the other hand, for low wind speed, viscous dissipation and dissipation due to slicks may be relevant processes in determining the shape of the gravity-capillary spectrum, again suggesting that not only the local wind speed determines the backscatter.

The above consideration prompted an extensive investigation into the dependence of the radar backscatter on physical parameters such as wind speed, sea state, the presence of slicks and even parameters such as the air-sea temperature difference. (The latter parameter becomes relevant when it is realised that the high-frequency wave spectrum depends on the surface stress and the relation between surface stress and wind speed at a certain height involves atmospheric stability (eg the air-sea temperature difference)). Thus, the VIERS-1 group[1] emerged which started an experimental study in the laboratory and at sea to address the above issues. Parallel to the experimental work, the VIERS-1 group started the development of a scatterometer algorithm based on the present understanding of the radar backscatter process and of the relevant processes governing the shape of the gravity-capillary spectrum. The observed results on radar backscatter and the short wave spectrum were used to tune a number of unknown parameters in the scatterometer algorithm. As a result, a backscatter algorithm based on physics rather than empirical fitting was obtained.

The next question to ask is whether the VIERS-1 scatterometer algorithm produces reliable results when applied on a global scale. Assuming that the ECMWF wind and wave fields are accurate, we determined the Radar backscatter with the VIERS-1 algorithm and compared the results with the backscatter as obtained from the ERS-1 satellite. The agreement between simulated and observed backscatter looks promising and

---

[1] VIERS-1 is a Dutch acronym for Preparation and Interpretation of ERS1 data. The project is a collaboration between the Royal Netherlands Meteorological Institute (KNMI), Delft Hydraulics, the Laboratory for Telecommunications and Remote Sensing Technology of Delft University of Technology, the University of Heidelberg, the Physics and Electronics Laboratory of TNO(FEL-TNO) and Rijkswaterstaat, Tidal Waters Division.

will be described in full detail in a forthcoming VIERS-1 report. Here, we shall only present the main result briefly, concentrating on some results obtained during the tuning of the VIERS-1 scat algorithms and on the sea state dependence of the backscatter.

2.1 Tuning the VIERS-1 backscatter algorithm

Using laboratory data for σ_o and the two dimensional wave number spectra, the performance of several backscatter models (*Fung*, 1987; *Holliday*, 1986; *Bahar*, 1981; two-scale approach (*Plant*, 1990)) was investigated. The two-scale model turned out to give satisfactory results in a reasonably short run time (VIERS-1 (1993)). Thus, the radar backscatter can be found by integrating the backscatter of the individual facets (which are tilted by the longer gravity waves) weighted with the probability that the water surface is tilted by a certain angle. For high wave numbers ($k>k_c$) the main scattering mechanism was assumed to be Bragg scattering, hence

$$\sigma_l \sim \Phi(k_b),\ k > k_c \tag{1}$$

while, for $k < k_c$, specular reflection was taken. Here, Φ is the wave number spectrum, k_R is the Radar wave number, θ_l is the local incidence angle which depends on the tilt of the water surface by the long waves and k_c denotes the separation scale between Bragg and specular reflection. Finally, k_b follows from the Bragg resonance condition between the electromagnetic wave and the surface waves and is given by

$$k_b = 2k_R \sin \theta_l \tag{2}$$

A complete account of this algorithm, including the choice of separation scale k_c is given in the VIERS-1 report (1993) (but see also *Plant*, 1990). The comparison given in the VIERS-1 report showed, however, that for low incidence angles the backscatter was overestimated. Wallbrink and Janssen ascribed this discrepancy to a too high value of the standard reflection coefficient (see also *Valenzuela*, 1978). By reducing it somewhat, they obtained the results as given in Fig 1. Indeed, an impressive agreement between simulated and observed backscatter, both for horizontal and vertical polarisation, is obtained, giving confidence in the electromagnetic part of the VIERS-1 algorithm.

The geophysical part of the VIERS-1 scatterometer algorithms is determined by the modules for the short wave spectrum and the module that gives the relation between wind speed at 10 m height, the air-sea temperature difference and the surface stress. We will not discuss the latter module as it is fairly standard, except that the surface roughness is sea state dependent and is given by the empirical expression from *Smith et al* (1992).

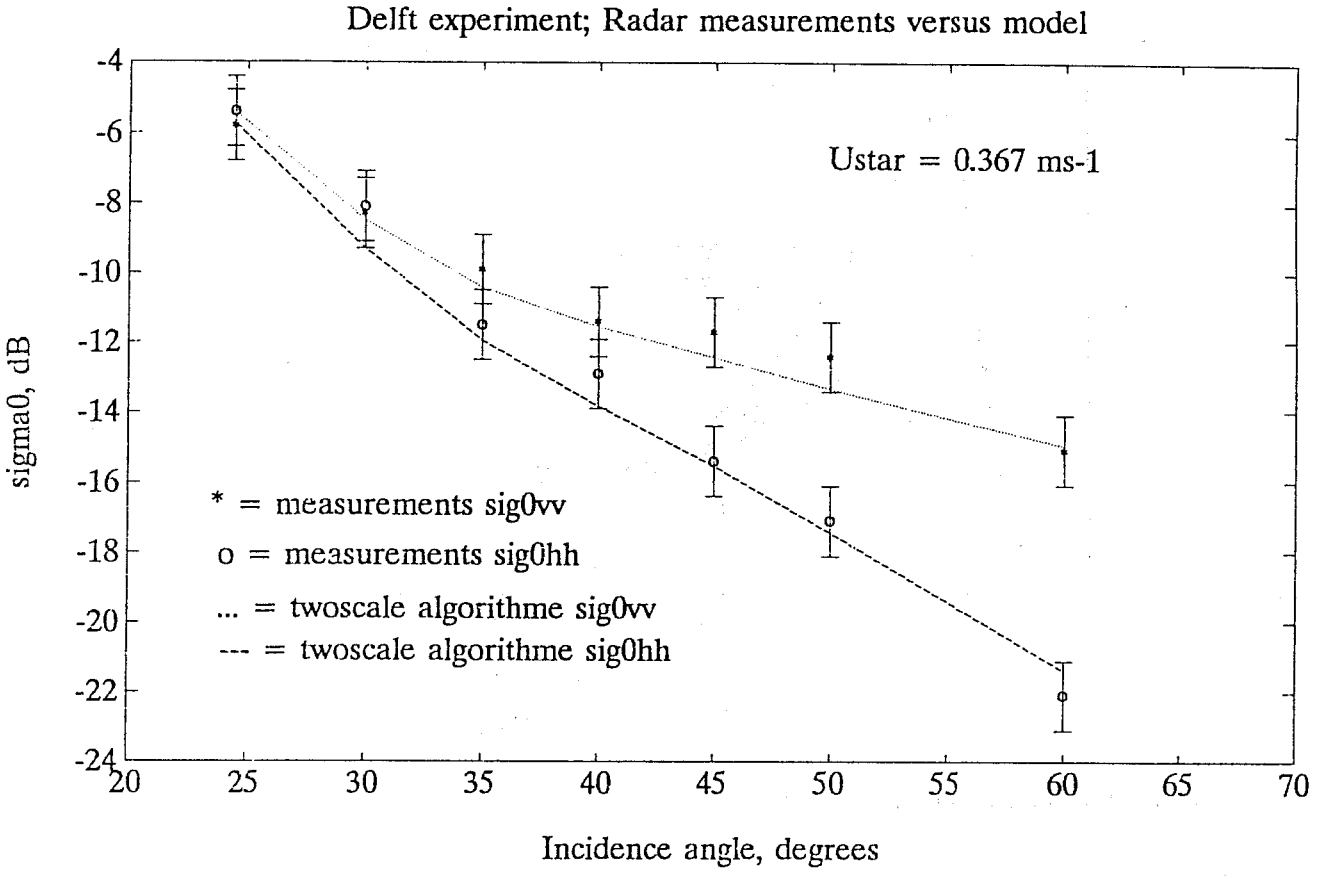

Fig 1 Comparison of simulated σ_o and observed σ_o as function of incidence angle.

The model for the short wave spectrum is based on the so-called energy balance equation, which is solved under steady state circumstances because the high-frequency waves have a very short response time scale. The energy balance equation for the short waves is therefore given by

$$\frac{\partial}{\partial t}\Phi = 0 = S_{in} + S_{nonl} + S_{visc} + S_{br} + S_{slicks} \tag{3}$$

where S_{in} represents the effect of wind, S_{nonl} describes the effect of 3 and 4 wave interactions, S_{visc} describes viscous dissipation, S_{br} describes dissipation due to white capping and S_{slicks} describes the resonant energy transfer between surface waves and slicks (Marengoni effect). The energy balance equation (3) is solved as a boundary value problem in wave number space by providing the energy flux from long to short waves at the boundary $k_{bou} = g/u_*^2$, corresponding to the condition $c/u_* = 1$ (where c is the phase speed of the waves and u_* the friction velocity). A pictorial view of the energy balance for short waves is given in Fig 2.

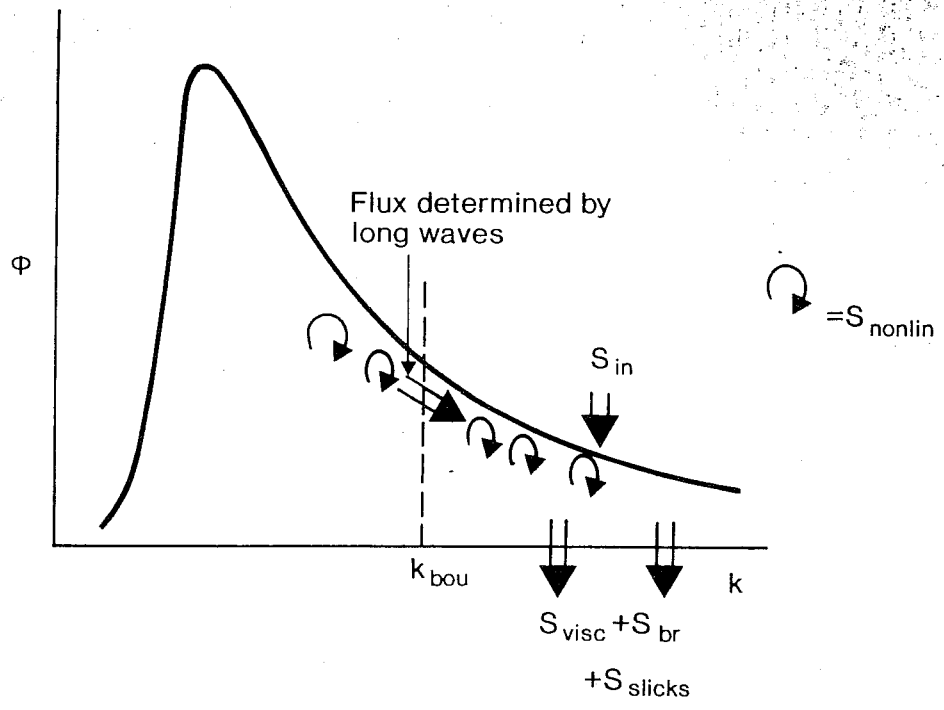

Fig 2 Pictorial view of the energy balance of short waves.

From this picture of the energy balance of short waves it is concluded that the gravity-capillary spectrum (and hence the backscatter) depends not only on the local friction velocity but also on parameters such as the stage of development of the long gravity waves. A complete account of the specific source terms used in the energy balance equation is given in VIERS-1 (1993). Here, we only present a comparison of simulated spectra and observed wind-wave tank spectra in Fig 3 to show that the present model is able to produce realistic spectra.

2.2 Evidence for wave-age dependence in scatterometry

(work done with P Woiceshyn)

Evidence of the possible dependence of the Radar backscatter on the state of the long gravity waves is hard to find. The reason for this is that a clear dependence on sea state can only be observed during rapidly varying conditions (front passages) involving swell and a significant wind sea. As on a global scale wind sea is only found in 10% of the cases, it is no wonder that evidence of sea state dependence is not easy to find. Nevertheless, *Davidson et al* (1993) investigated during the NORCSEX ERS-1 pre-launch experiment of March 1988 the passage of a front and they found that the wind forcing dependence of the backscatter was less during swell-dominated than for developing wind-wave conditions. This, therefore, suggests a sea state dependence of the backscatter.

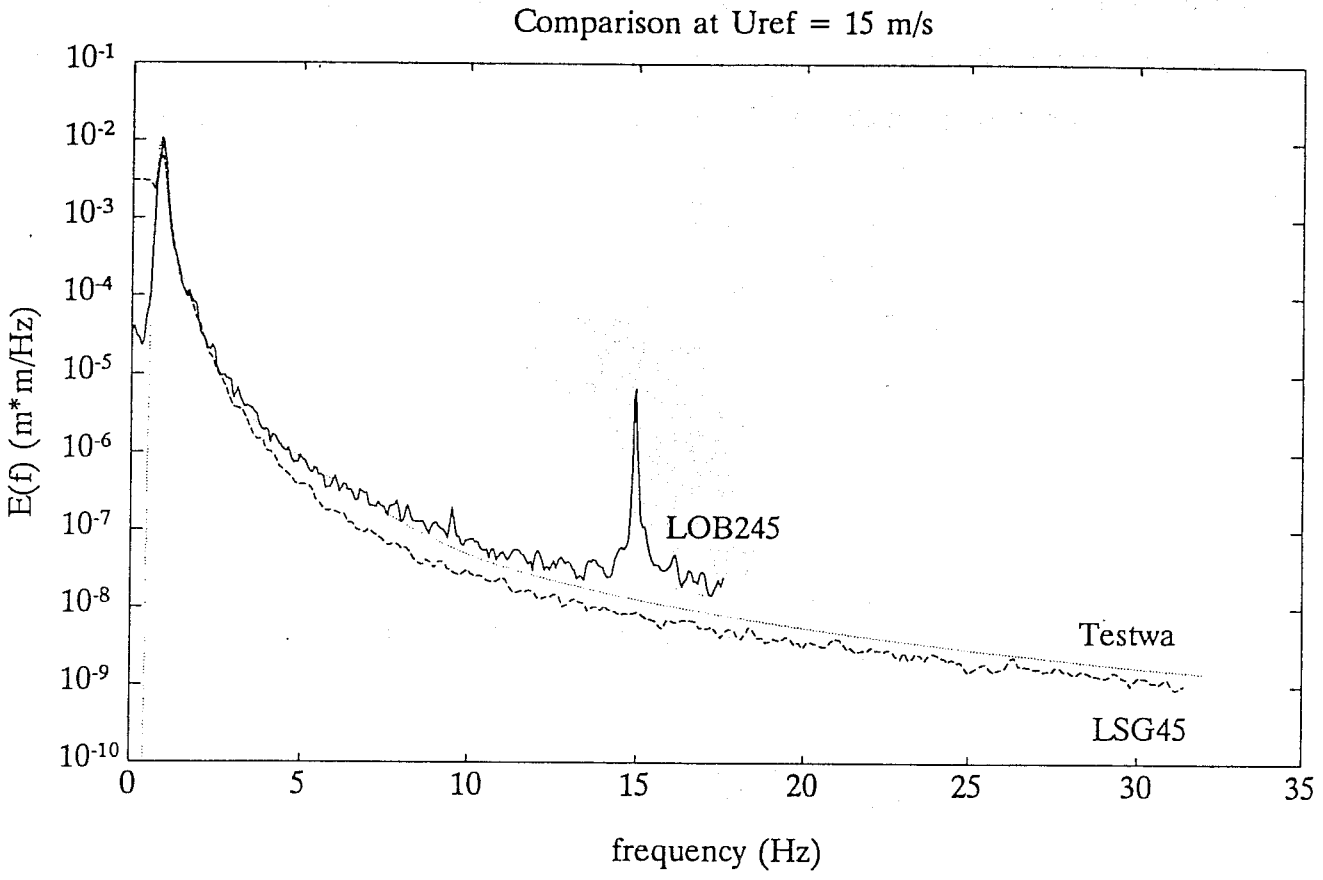

Fig 3 Comparison of simulated and observed short-wave frequency spectra for a fetch of 90 m.

Let us try to quantify what is meant with the sea state in this context. In principle, the sea state is completely specified by means of the two-dimensional wave spectrum. In practice, one would like to use a single parameter to quantify the sea state and therefore the complete two-dimensional spectrum is not a convenient measure to work with. From *JONSWAP* (1973) we know, however, that in case of wind sea such a sea state parameter exists. It is called the wave age and it is defined as

$$\xi = c_p/u_* \tag{4}$$

where c_p is the phase speed of the peak of the spectrum ($c_p = g/\omega_p$, $\omega_p = \sqrt{gk_p}$; here ω_p is the peak angular frequency) and u_* the friction velocity. Typically, values of the wave age ξ range from $\xi = 5$ ('young' windsea) to $\xi = 25$ ('old' wind sea). Thus, if the wave age ξ is known, the gravity wave spectrum for wind sea may be constructed so that the sea state is now known. It should be pointed out that the characterisation of the sea state for wind sea by a single parameter is possible because the waves are then so steep that nonlinear 4 wave interactions are dominant in shaping the spectrum, hence the spectrum is (quasi) universal.

Let us now return to the energy balance for the short waves (cf Section 2.2). Similarly, since for wind sea the waves are steep, it may be argued that even for the short waves the nonlinear 3 and 4 wave interactions

are dominating the energy balance, thus, to a large extent, the short wave spectrum is determined by the wave age parameter ξ. It is therefore tempting to investigate the dependence of a backscatter algorithm on the wave age parameter ξ. In other words, for wind waves one would expect a relation between the

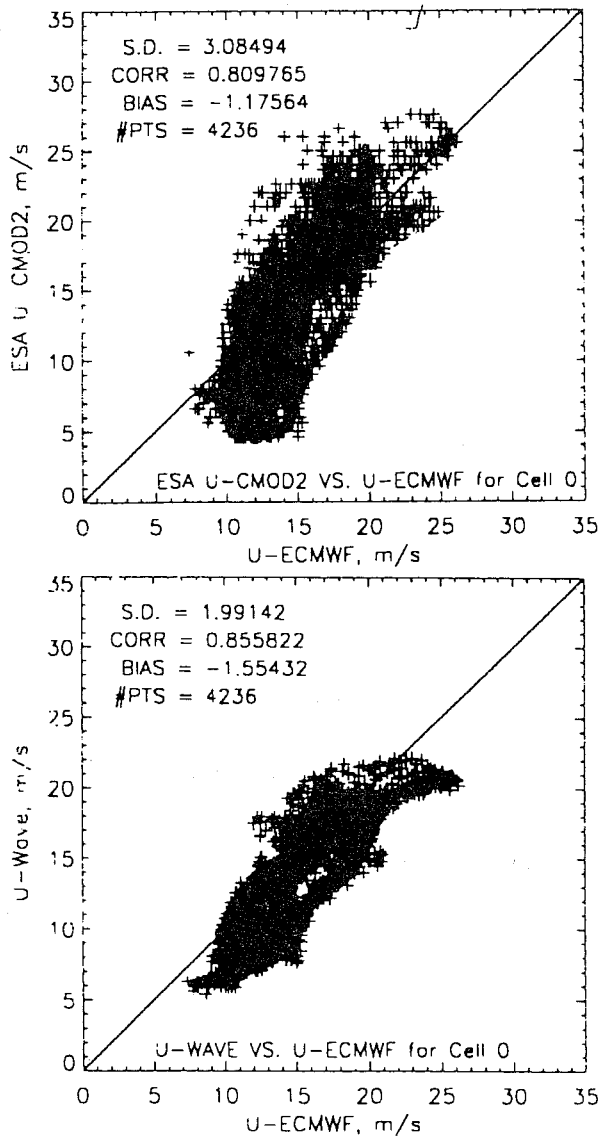

Fig 4 Comparison of simulated and analysed wind speed. Top panel: CMOD2; Bottom: wave age dependent algorithms.

backscatter σ_o and ξ. In order to determine a possible dependence on wave age, we therefore collocated peak phase speeds c_p from the third generation WAM model running at ECMWF with the ERS-1 files prepared by Ad Stoffelen and Ross Hoffman that include the ECMWF analysed winds and the CMOD2 winds obtained from the ERS-1 scatterometer data. Let us call the CMOD2 wind speed U_{scat}. In view of the above we give, however, a slightly different interpretation to the parameter U_{scat}; we assert that

$$U_{scat} \sim \xi^{-1} \tag{5}$$

Then, from U_{scat} and the phase speed c_p we obtain the friction velocity u_*,

$$u_* = 0.0022\, c_p U_{scat} \tag{6}$$

and this is converted to 10 m wind speeds using a sea state dependent roughness length formulation obtained during HEXMAX (*Smith et al*, 1992),

$$z_0 = \beta u_*^2/g,\ \beta = 0.48 u_*/c_p \tag{7}$$

while for low winds the usual viscous roughness length was used. Thus

$$U_{10} = \frac{u_*}{\sqrt{C_D}},\ C_D = (\kappa/\ln(10/z_0))^2 \tag{8}$$

where κ is the von Karman constant ($\kappa = 0.41$). The wind speed obtained in this manner was compared with the analysed ECMWF wind speed. Considering only cases of wind sea with wave age $\xi<25$, the wave age dependent algorithm gives a higher correlation with the ECMWF wind speed than the traditional CMOD2 algorithm (see Fig 4).

This suggests that there is potential in the use of wave age in scatterometry. However, it should be pointed out that this is certainly not the whole story. In agreement with the work of the VIERS-1 group, it is expected that, in order to obtain a reliable retrieval algorithm, the short wave spectrum would have to be determined explicitly, including its dependence on environmental parameters such as slicks, air-sea temperature difference, etc (which are all important for low winds). We shall therefore investigate the performance of the VIERS-1 scatterometer algorithm in the next section.

2.3 Validation of VIERS-1 scatterometer algorithm against ERS-1 data

(work done with H Wallbrink and J Janssen)

After our excursion to the problem of the possible dependence of the Radar backscatter on the sea state we would like to return now to the question of the application of the VIERS-1 scat algorithm to the simulation of the backscatter σ_o under realistic circumstances.

It is emphasised that this question is a valid one because so far the VIERS-1 scat algorithm has only been validated under the limited conditions of the laboratory. In addition, the Radar in the laboratory was X-band, while the Radar on board of ERS-1 is C-band.

Using the collocation files mentioned in Section 2.2 we determined with the VIERS-1 scatterometer the Radar backscatter σ_o (vertical polarisation). The air-sea temperature difference was set to zero since neutral

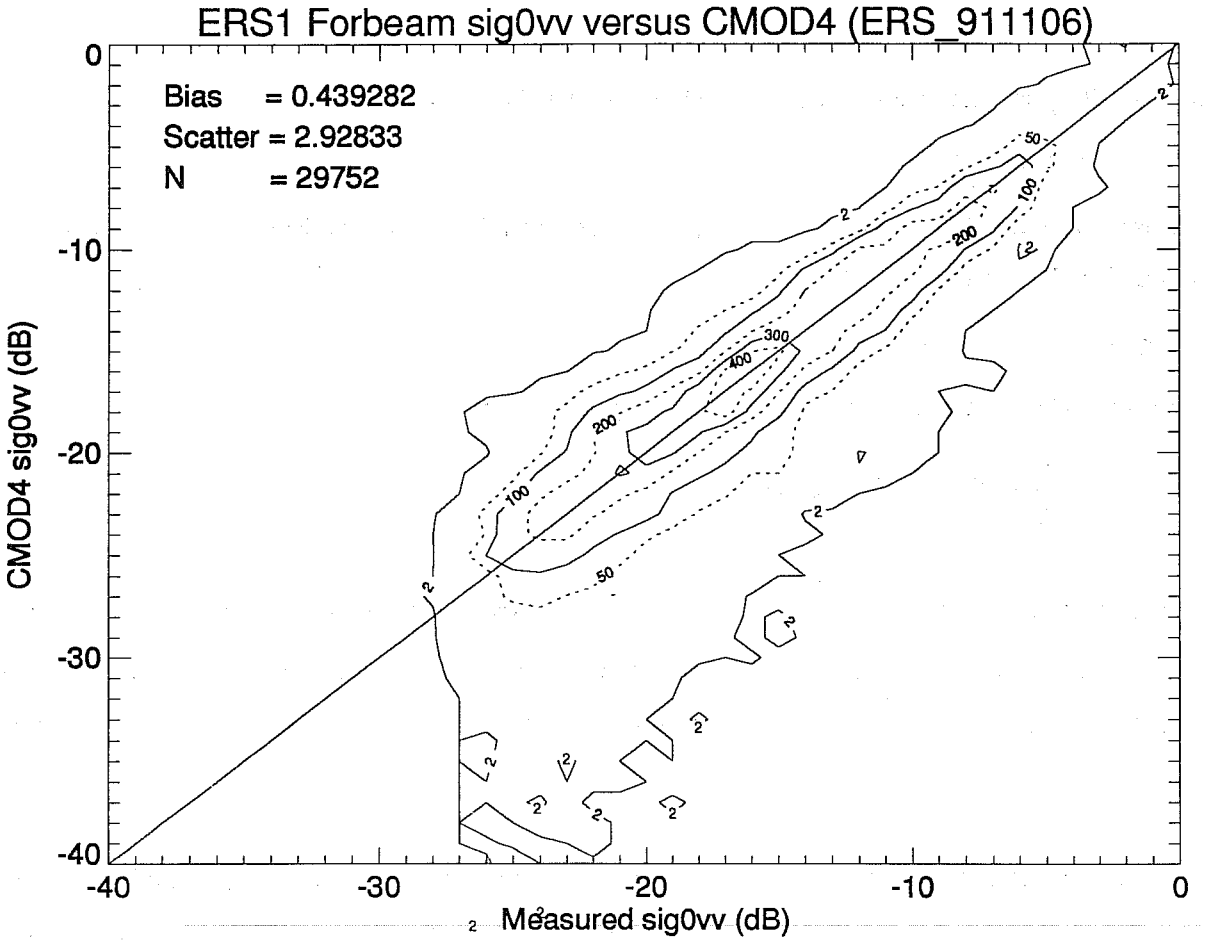

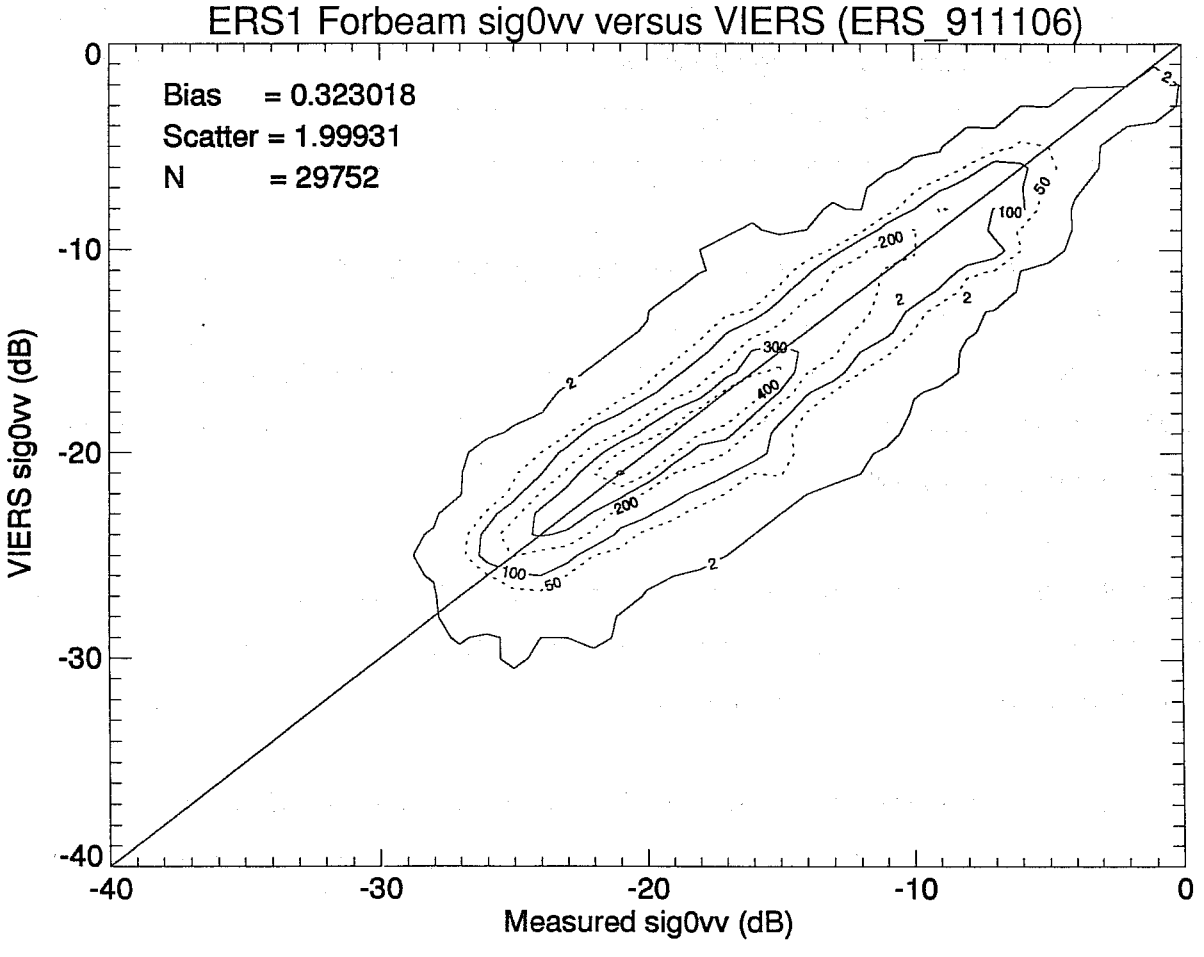

Fig 5 Comparison of simulated and observed σ for CMOD4 and VIERS.

stability is the most common situation that occurs over the oceans. In Fig 5 we compare the simulated backscatter with the observed ones showing an overall good agreement, even for low wind speed. As a bench mark, we have also shown results of the present operational scatterometer algorithm CMOD4.

We conclude from this comparison that the VIERS-1 scatterometer algorithm, based on our present knowledge of air-sea interaction, is performing well, even compared to CMOD4 which is tuned on the data set we have considered in this comparison. The advantage of the VIERS-1 algorithm over CMOD4 is, however, that it is based on physics so that dependencies on sea state, slicks, etc are automatically included in the algorithm. One would therefore expect that this algorithm is performing better in rapidly varying circumstances, such as the passage of frontal systems. In order to substantiate this claim, the VIERS group is presently working on the inversion of the VIERS-1 scatterometer algorithm so that a retrieval of wind speed and wind direction from observed back scatter returns becomes feasible.

3. IMPLEMENTATION AND VALIDATION OF A COUPLED WIND-WAVE MODEL

(work done together with P Viterbo and A Beljaars)

During the past ten years there has been much interest in the problem of the interaction of wind and waves with emphasis on the dependence of the momentum transfer across the air-sea interface. The common belief in the field of air-sea interaction was that air turbulence was the major mechanism to maintain the wind profile and the effect of surface gravity waves was regarded to be small. Thus, in effect the interaction between wind and waves was regarded as a one-way street, which enabled wave modellers to force their wave model with given wind fields (from an atmospheric model eg). Experimental evidence collected in the 1980's (*Donelan*, 1982; *Maat et al*, 1991; *Smith et al*, 1992) showed, however, that this picture of the interaction of wind and waves was not complete. It was found that, especially for young wind sea (this state occurs eg near the coast for off-shore winds or near fronts), the airflow depends on the sea state. This suggested that it would be more appropriate to regard the interaction process of wind and waves as a two-way street.

Parallel to this development a theory of the two-way interaction of wind and waves was developed, giving the sea state dependence of momentum, heat and moisture transfer both for pure wind sea and mixed wind sea, swell cases (*Janssen*, 1982; *Janssen*, 1989; *Janssen*, 1991). A parametrized version of the theory for momentum transfer is included in the latest cycle of the WAM model. Simulations with the WAM model show that depending on the sea state, the drag coefficient may vary by a factor of two. Therefore, one may wonder whether two-way interaction has impact on the analysis of air-sea fluxes and on eg the evolution of depressions. Here, we will concentrate on the dynamical aspects first, leaving, as planned, the issue of analysed fluxes to the next stage in the project. We therefore performed numerical experiments with a coupled ocean-wave, atmosphere model to investigate impact of two-way interaction on medium-range weather forecasting. Results so far show a small beneficial impact in case a significant storm is present. Typically, we found that the period over which deviations from the reference run (ie one-way interaction) occurred was about 5-7 days. This is about the time scale to have a significant impact of surface friction on the evolution of a depression. One would therefore expect a more substantial impact on the climate of the model. And indeed, the main point of this report is to show that inclusion of the effect of ocean waves on the air-sea momentum transfer has a significant impact on the atmospheric circulation. Also, the climate of parameters such as wind speed, wave height and surface stress changes significantly.

The plan of the remainder of this report is as follows. First, we briefly describe the effect of ocean waves on momentum, heat and moisture transfer. Next, we discuss how we coupled the ocean-wave WAM model with the atmospheric ECMWF model and we compare numerically simulated roughness length with field data from HEXOS (*Smith et al*, 1992). The rest of the report is then devoted to the impact of two-way interaction on large-scale processes in the atmosphere. We then first describe possible impact on 10 day

forecasts and, next, we discuss our results of seasonal runs over a period of 90 days. In passing, we point out the well-known need of Monte Carlo forecasting and we conclude by showing that two-way interaction has a significant impact on the atmospheric circulation. The resulting changes in momentum flux are found to be considerable which we judge from the large differences in surface elevation one obtains by forcing a barotropic ocean circulation model with surface stresses from the two-way interaction run and the reference run.

3.1 Two-way interaction of wind and waves

During the past decade a considerable amount of evidence has been collected on the sea state dependence of the momentum transfer at the air-sea interface (*Donelan*, 1982; *Maat et al*, 1992; *Smith et al*, 1993). In these studies the dray coefficient C_D or the roughness length z_o was parametrized in terms of a single parameter, namely the wave age $\xi = c_p/u_*$, in order to describe the sea state dependence of the momentum transfer. An example of such an empirical fit is given in Eq (7). However, we know (see eg the discussion in the previous section) that a characterisation of the sea state by means of a single parameter only works for pure wind sea. A parametrization that is also valid for mixed wind sea, swell situation (the most common circumstance on the ocean) was proposed by *Janssen* (1991). The wave age ξ is then replaced by the so-called wave-induced stress τ_w.

Starting from his earlier work on the quasi-linear theory of wind-wave generation (*Janssen*, 1989), the neutral drag coefficient over ocean waves was given as

$$C_D = \left\{ \frac{\kappa}{\ln(L/z_o)} \right\}^2 \tag{9}$$

where L is a reference height (typically, $L \sim 10$–$30\ m$), κ the von Karman constant and z_0 the roughness length, given as

$$z_0 = \frac{\beta u_*^2}{g},\ \beta = \alpha/[1-\tau_w/\tau)^{1/2} \tag{10}$$

where u_* is the friction velocity ($\tau = u_*^2$) and $\alpha = 0.01$. The Charnock parameter β depends on the sea state through the wave-induced stress τ_w defined as

$$\vec{\tau}_w = \int d\vec{k}\ \omega\ \frac{\vec{k}}{k}\ S_{in}(\Phi) \tag{11}$$

where the wave spectrum Φ follows from the energy balance equation

$$\frac{\partial}{\partial t}\Phi + \frac{\partial}{\partial \vec{x}}(v_g \Phi) = S_{in} + S_{nl} + S_{diss} \tag{12}$$

which is solved by the third generation WAM model (*WAMDI*, 1988). Here, v_g is the group velocity ($\vec{v}_g = \partial\omega/\partial k$) and the source terms describe the physics of the generation of surface waves by wind (S_{in}), nonlinear interactions (S_{nl}) and dissipation due to white capping.

For small wind speed, on the other hand, we take the viscous roughness length (v_a is the kinematic viscosity of air)

$$z_o = 0.1\ v_a/u_* \tag{13}$$

assuming that the air flow is laminar in those circumstances and obeys the law of the wall. We will see that the inclusion of the viscous roughness length will give significant differences in the tropics, eg, where the wind speed is usually quite low.

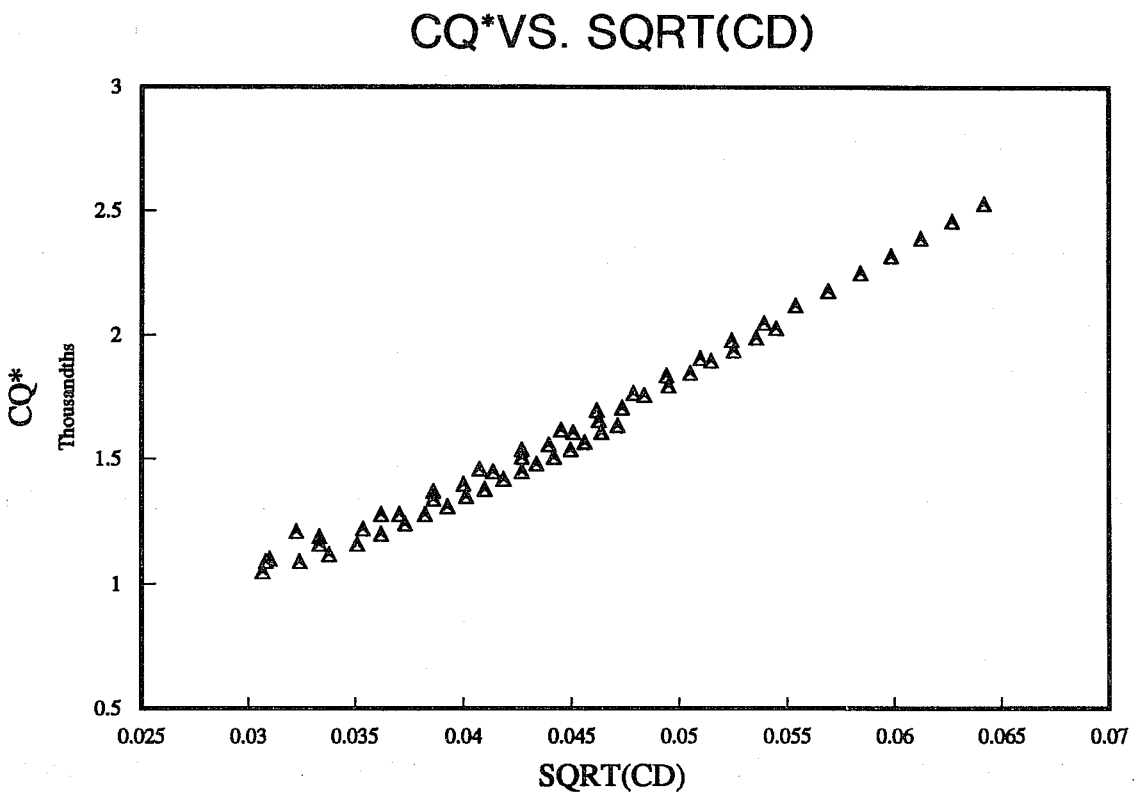

Fig 6 Dependence of Stanton number C_{q*} on the drag coefficient C_D.

Heat and moisture exchange across the air-sea interface can be treated in a similar manner. For the heat flux q_* we find in the so-called passive scalar approximation

$$q_* = C_{q*}\ U(L)\ \Delta T(L), \tag{14}$$

where $\Delta T(L)$ is the air-sea temperature difference at height L, U the wind speed and the so-called Stanton number is given as

$$C_{q*} = C_D^{1/2}\tilde{C}_{q*}^{1/2} \tag{15}$$

Here, $\tilde{C}_{q*}$ (which is related to the temperature profile) is virtually independent of wind speed or sea state, hence, C_{q*} is proportional to $C_D^{1/2}$ (see Fig 6) in agreement with work of *De Cosmo* (1991).

Since the moisture exchange behaves in a similar fashion as heat transfer it is concluded that these processes are less sensitive to changes in the sea state (and the wind) than the momentum transfer.

3.2 A coupled ocean-wave, atmosphere model

After having discussed the physics of air-sea interaction, we now turn our attention to some of the large-scale consequences of two-way interaction, ie we consider the impact of ocean waves on the atmospheric circulation on timescales ranging from the medium range (10 days) to seasonal timescales (90 days).

Following *Weber et al* (1993), we have developed a scheme to couple an ocean-wave and atmospheric model (WAM-ECMWF), a schematic view of which is presented in Fig 7. In words, we run the atmospheric model for 1 hour, then

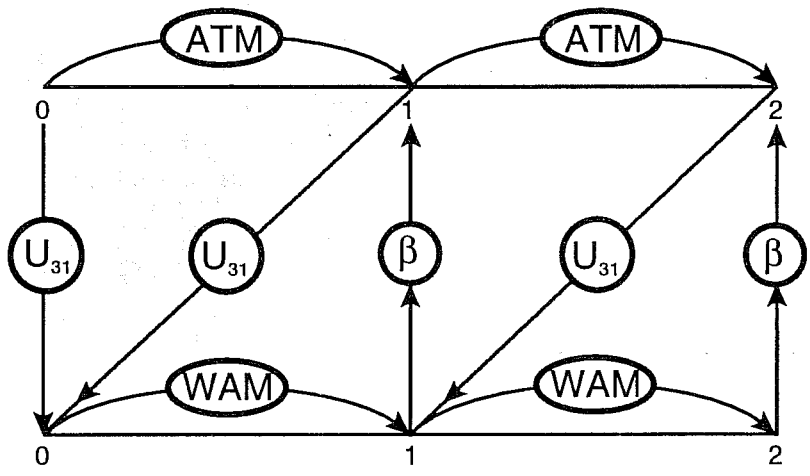

Fig 7 Schematic of coupled system

a wave forecast is run using the winds produced by the atmospheric model and finally the atmospheric model is run for another hour, now using the Charnock parameter, that has been determined by the WAM model in the previous cycle, for the momentum transfer. In the present set-up we have taken the neutral exchange coefficients for momentum, heat and moisture to be identical since this is a basic assumption in cy44 of the ECMWF model. Further experiments where we will use the exchange coefficients for heat and moisture as given in section 3.1 are planned to take place in the near future.

In the remainder of this report we shall discuss the impact of two-way interaction on the atmospheric circulation. We measure this impact by comparing results of two-way interaction with results of one-way interaction experiments. The one-way interaction experiments are performed with the same software as the two-way experiments except that in the one-way experiment, which we call the control experiment from now on, the Charnock parameter takes the constant value 0.018, while in the two-way experiment (coupled for short) the Charnock parameter is determined from the wave model, thus giving a consistent energy balance at the surface.

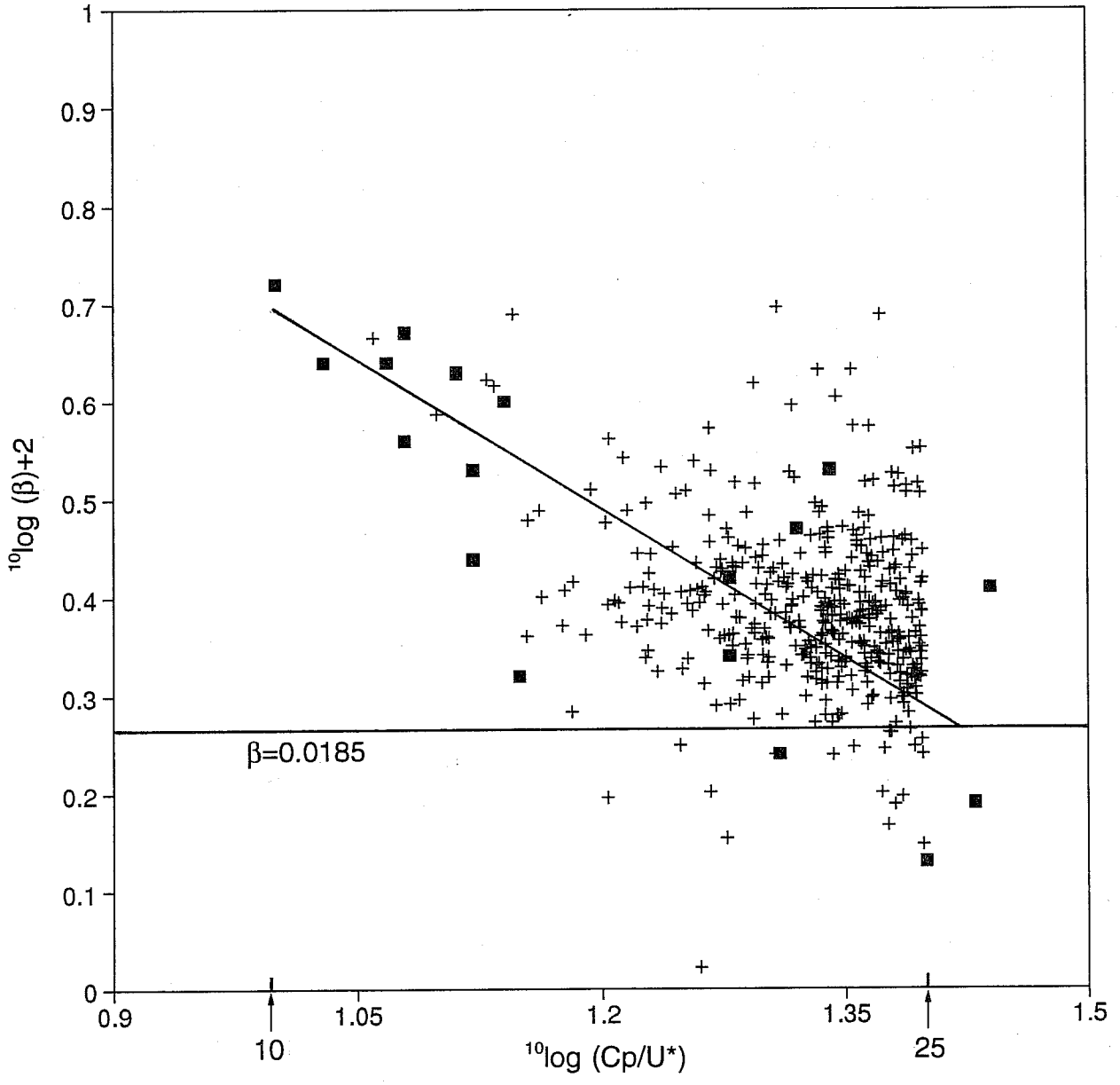

Fig 8 Simulated (+) and observed (■) Charnock parameter. The usual Charnock constant $\beta = 0.0185$ and the *Smith et al* (1992) fit are given as well.

Before we discuss our results of a number of 10 day forecasts and seasonal forecasts with this coupled system, we compare, first of all, the numerically simulated Charnock parameter with data obtained during HEXOS (see Fig 8). We have also displayed Eq (7) which is the mean result of *Smith et al* (1992). As HEXOS data relate to wind sea data we selected only those simulated roughness lengths from an arbitrary date that satisfied according to the WAM model the condition for wind sea, ie $\xi = c_p/u_* < 25$. In Fig 9 we have shown the drag coefficient C_D for the same date as a function of wind speed. As a reference, we also show the drag coefficient of the standard ECMWF model which is based on a Charnock relation with Charnock constant $\beta = 0.018$. Clearly, there are significant differences between drag as determined from the two-way interaction scheme and the standard Charnock relation and the question now is to what extent

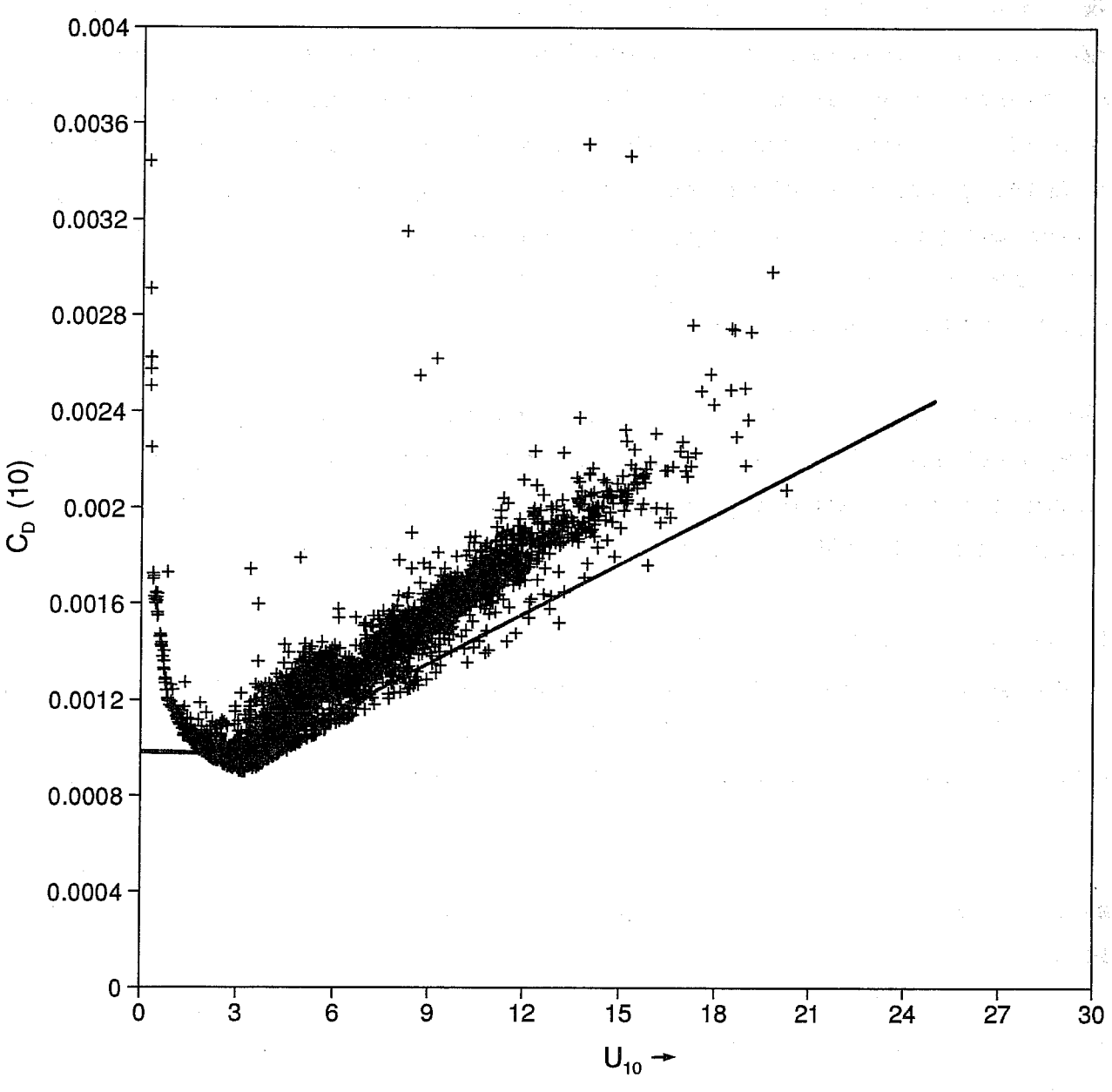

Fig 9 Simulated drag coefficient (+) as function of wind speed at 10 m height. The full line is the present ECMWF parametrization for C_D.

this will affect medium-range and seasonal forecasting. The remainder of this report will be devoted to answering this question.

3.3 Ten day forecasts

We have performed an extensive set of 10 day forecasts on randomly selected cases and on cases where a significant storm was present at day 2 of the forecast. The first set of experiments showed that two-way interaction had no impact on scores such as the anomaly correlation, while in the case of a severe storm, a small beneficial impact was found over areas such as the Pacific and North America.

Let us discuss results of 10 day forecasts of 'randomly' selected cases first. The starting date was the fifteenth of every month, between October 1991 and September 1992 so we have twelve forecasts. The initial data for the atmospheric fields were taken from the analysis produced by the atmospheric model which was operational at the start date of the forecast. No initial data for the WAM model were available because the wave spectra have not been archived so far. The wave model was therefore started with a JONSWAP spectrum 5 days before the starting data of the two-way interaction forecast and was integrated until the starting date of the experiment by forcing it with analysed winds from the ECMWF archive. This warm up period of 5 days is sufficient to generate realistic wind seas but is too short for giving realistic swell in the tropical areas for instance.

The quality of a forecast is usually judged by means of a comparison with the verifying analysis. We will show plots of the rms difference between forecast and analysis and the so-called anomaly correlation which measures the correlation between forecast and verifying analysed deviation from climate. When the anomaly correlation drops below 60% the forecast is usually regarded to be of little use.

In Figs 10a-10e we show the mean over the 12 cases of the anomaly correlation and rms error of the 1000 mb geopotential of 6 areas, namely Europe, Northern Hemisphere, Southern Hemisphere, Tropics and the North Pacific. There are differences, but they are small and occur late in the forecast, typically after day 5, when the scores drop below the significant level. We will discuss the long time scale for impact in a while.

Another way of measuring differences is to compare directly with observations instead of with an analysis. Fortunately, during the period of interest, altimeter wind speed and wave height data from ERS-1 were available. Using collocation software provided by Björn Hansen we could verify the quality of the 5 day forecast. The statistics for 5 forecasts are shown in Table I. Incidentally, the reason for choosing the 5 day forecast is that at day 5 one hopes to see some differences between coupled and control run.

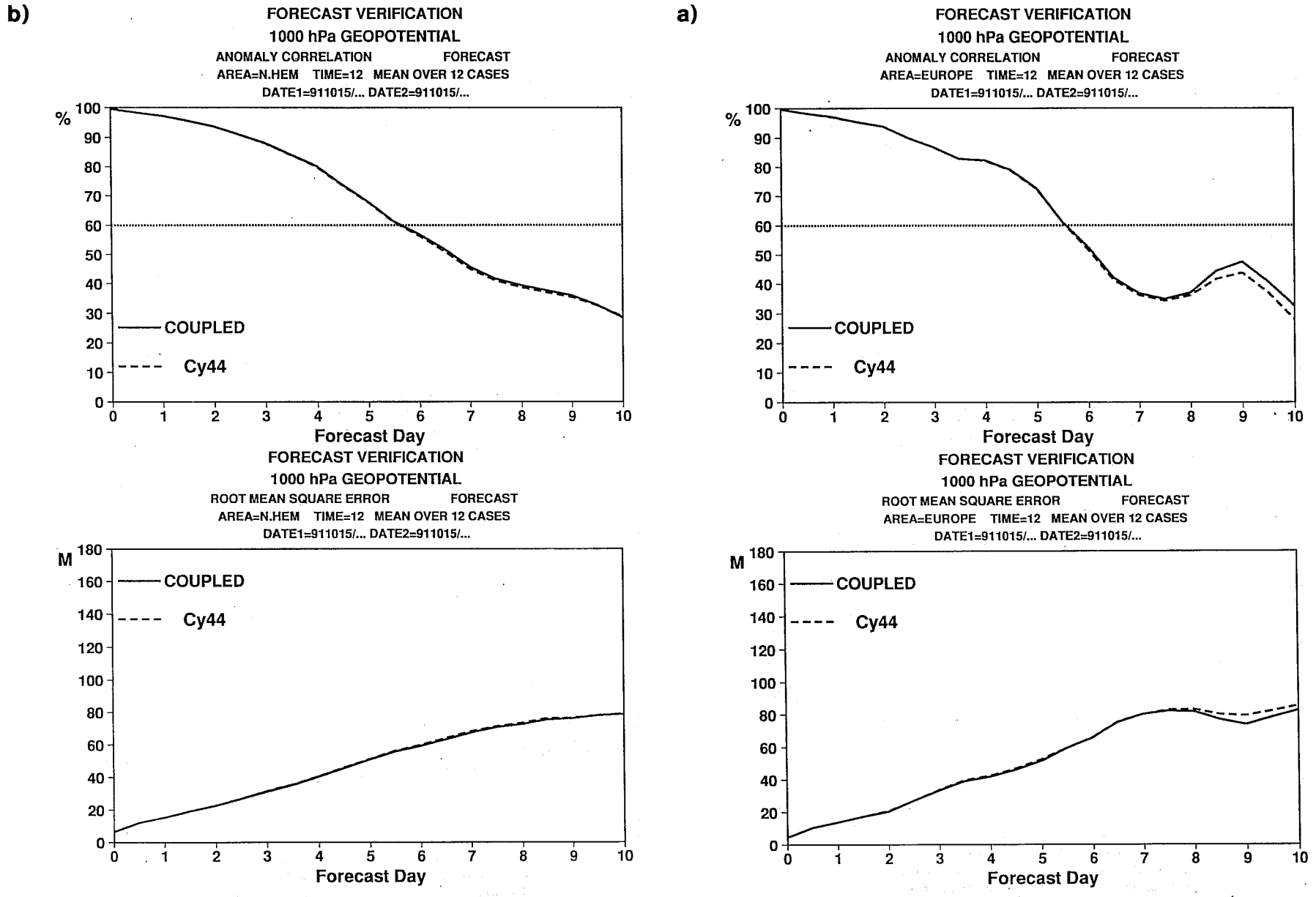

Fig 10 Anomaly correlation coefficient and RMS error of 1000 hPa geopotential height for (a) Europe, (b) Northern Hemisphere, (c) Southern Hemisphere, (d) Tropics and (e) North Pacific.

d)

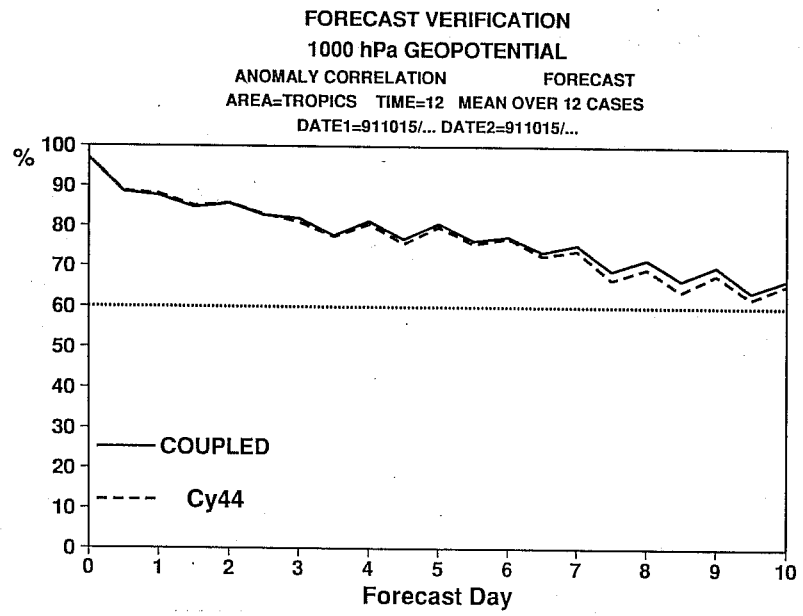

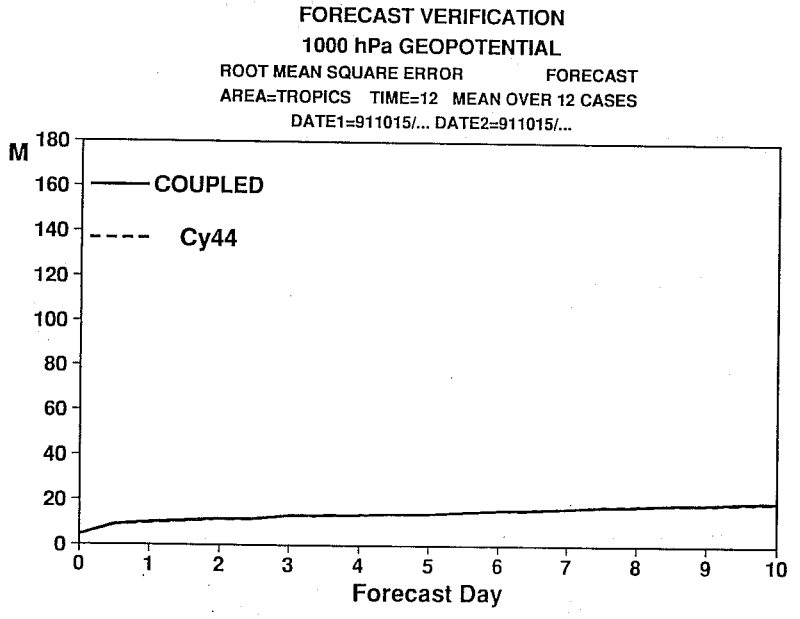

Fig 10 Continued.

c)

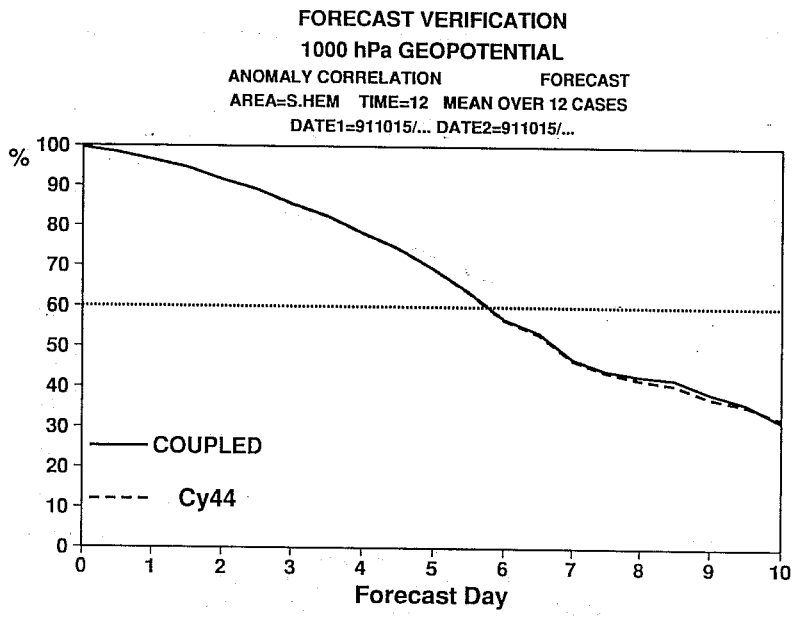

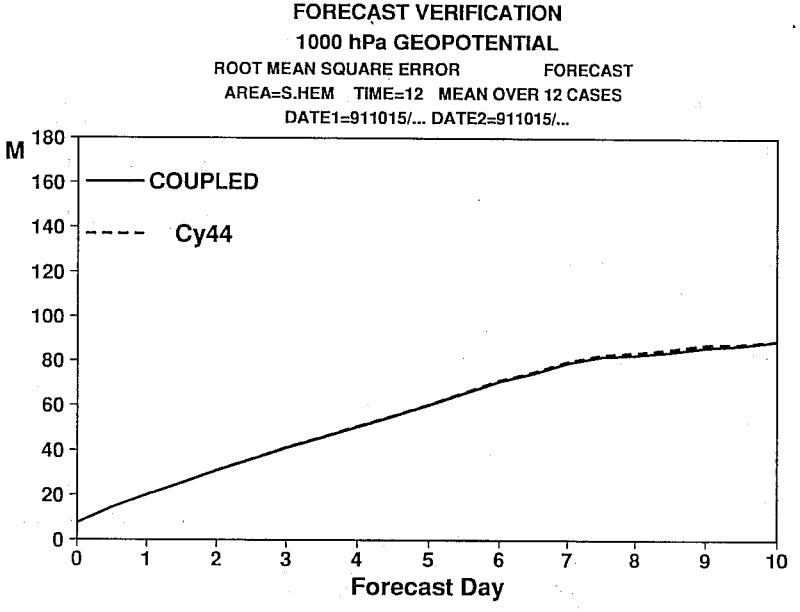

e)

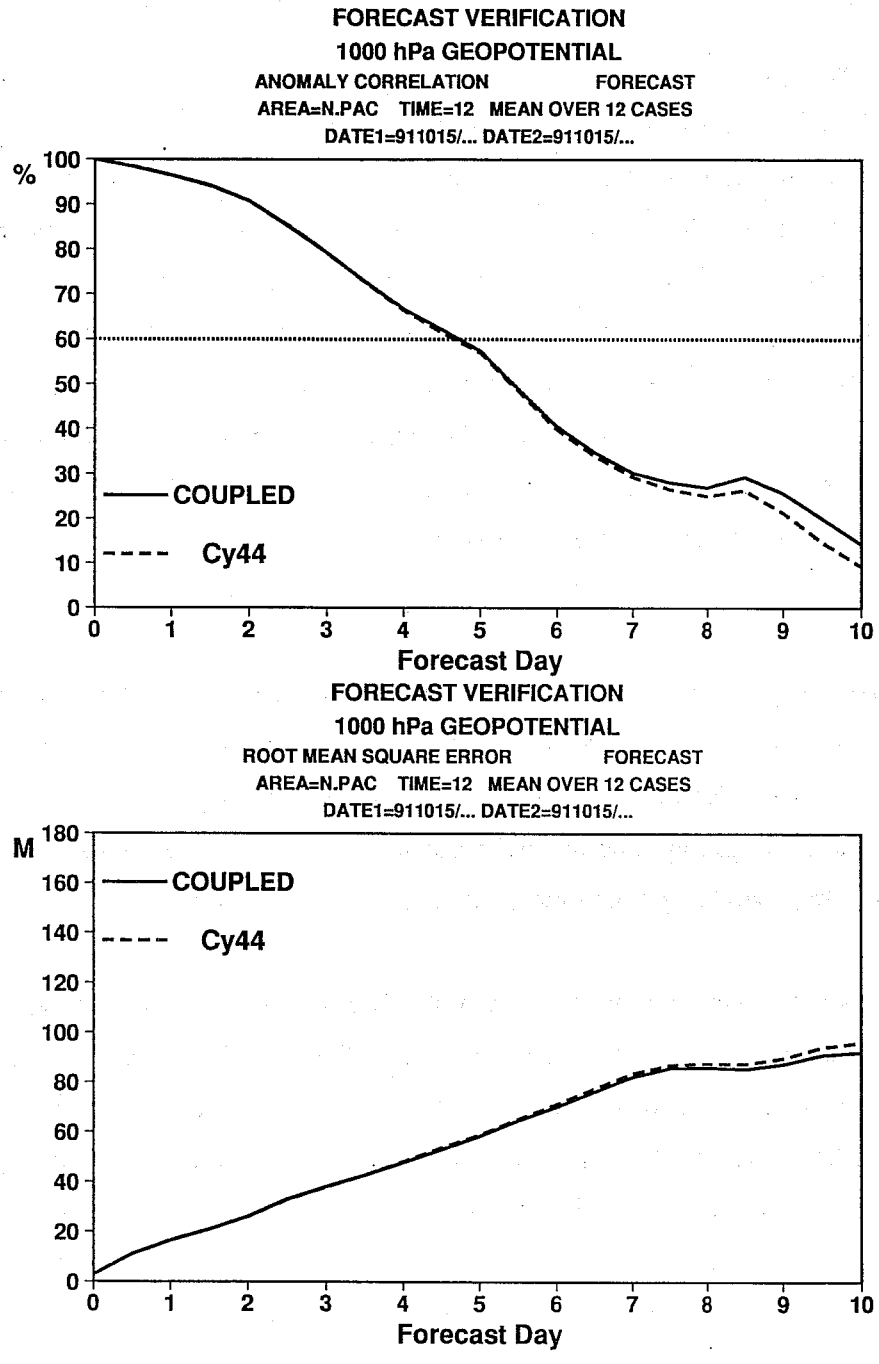

Fig 10 Continued.

	Coupled				Control			
	H_s (m)		U_{10} (m/s)		H_s (m)		U_{10} (m/s)	
	BIAS	SD	BIAS	SD	BIAS	SD	BIAS	SD
911115	-0.46	0.71	2.7	2.55	-0.40	0.73	2.78	2.58
920115	-0.40	0.61	-0.05	2.94	-0.33	0.64	0.04	2.96
920315	-0.54	0.66	0.53	3.01	-0.48	0.69	0.60	3.01
920515	-0.78	0.54	-0.54	3.14	-0.72	0.54	-0.52	3.16
MEAN	-0.48	0.65	1.02	2.83	-0.42	0.68	1.09	2.85

Table 1 Global verification of forecast at day 5 for wave height and surface wind speed at 10 m height. Bias is the difference of model and ERS-1 observation.

Let us discuss the wind speed statistics first. Apart from November 1991, results for the bias in wind speed look quite good for both coupled and control. The reason that November 1991 is exceptional is related to a bias in the wind speed algorithm of the ERS-1 Radar Altimeter. This bias was discovered by collocation of ERS-1 wind speeds and ECMWF wind speeds and the ERS-1 wind speed algorithm was corrected for this at the end of 1991. If one would omit the exceptional November 1991 case, then the overall bias in wind speed would be reduced considerably. The bias from the coupled run becomes -0.007 m/s while the bias from the control run becomes 0.07 m/s which, in view of an overall standard deviation of about 2.8 m/s, may be regarded as quite small. In fact, the bias for the control run is just statistically significant, as far as the verification with altimeter data is concerned. The wind speed bias between coupled and control run is just significant; on average, at day 5, the coupled wind speed is somewhat slower than the control wind speed.

Regarding the wave height statistics, it should be noted that the standard deviation is quite low (± 0.65 m) while evidently both models are underpredicting the wave height by about 0.45 m. Compared to the operational WAM model which has a typical bias of 10 cm, this bias may be regarded as high. The reason for this is simply that the spin up time for the WAM model is too short so that swells in eg the tropical areas are too low. In general a spin up time of about three weeks is needed.

Our overall impression is therefore that at day 5 in the forecast both the coupled model and the one-way interaction version are doing a reasonable job. Both regarding wave height and wind speed, the coupled model gives lower mean values, while the standard deviation is slightly lower for the coupled run. In addition, it should be pointed out that, apart from the smallness in differences, it is a very difficult task to decide which of these models are better in a comparison with altimeter data since the retrieval algorithms for wind speed and wave height of the ERS-1 Radar Altimeter have been tuned using operational results of the stand-alone version of the ECMWF model (wind speed) and the WAM model (wave height) [this corresponds to what we termed one-way interaction].

There is no doubt that differences will grow with forecast time. To illustrate this we show in Fig 11 the wind speed differences of day 4 and day 8 in the forecast of 15 January 1992. Contours are plotted every ½ m/s and dots indicate a positive difference between coupled and control run. Evidently, the differences in wind speed at day 8 are large scale and rather big (see eg in the North Atlantic and North Pacific). However, when collocated with the Altimeter data of that day the difference in bias between coupled and control run is only 13 cm/s. The corresponding scatter diagram of coupled wave height and wind speed at day 8 is shown in Fig 12. These diagrams illustrate a well-known feature that during a forecast the scatter in wind speed is much larger than the scatter in the wave height. There are two reasons for the reduced scatter in wave height. First of all, at a global scale 80% of the sea states are mainly swell that has been

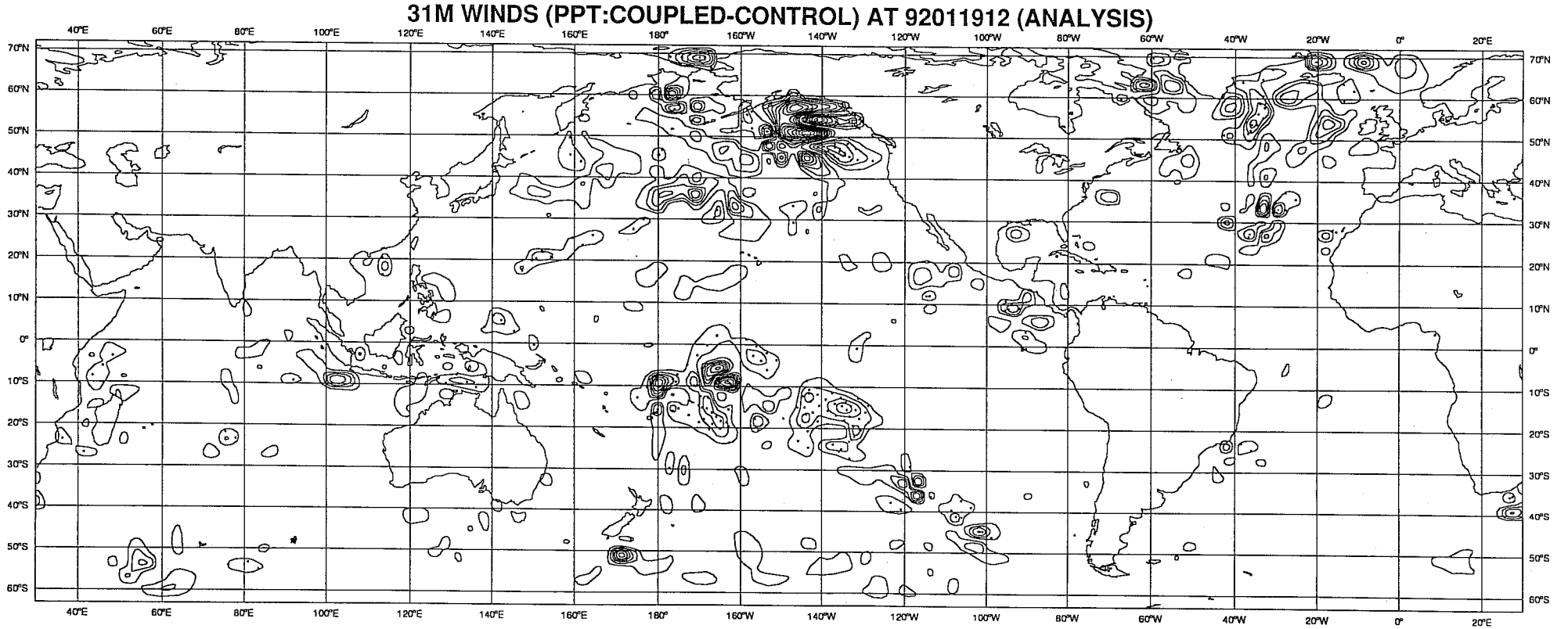

Fig 11a Wind speed differences at day 4 of the forecast of 15 Jan 1992. Contours every 0.5 m/s. Dots denote positive differences.

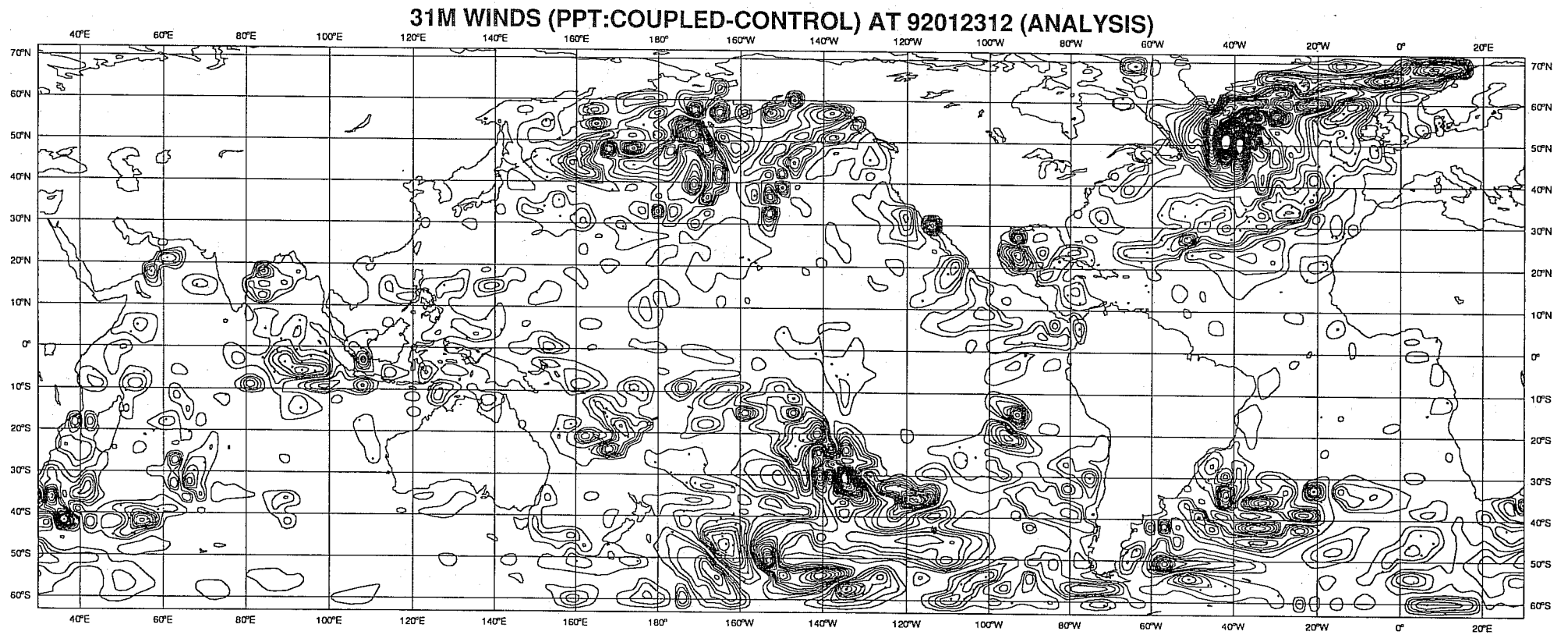

Fig 11b Wind speed differences at day 8 of the forecast of 15 Jan 1992. Contours every 0.5 m/s. Dots denote positive differences.

WAM–Model – ERS–1 – Comparison (ppt)
Radar – Altimeter – Waveheights
period from 01/22/1992 16:06'37" to 01/23/1992 08:25'39"
GLOBAL

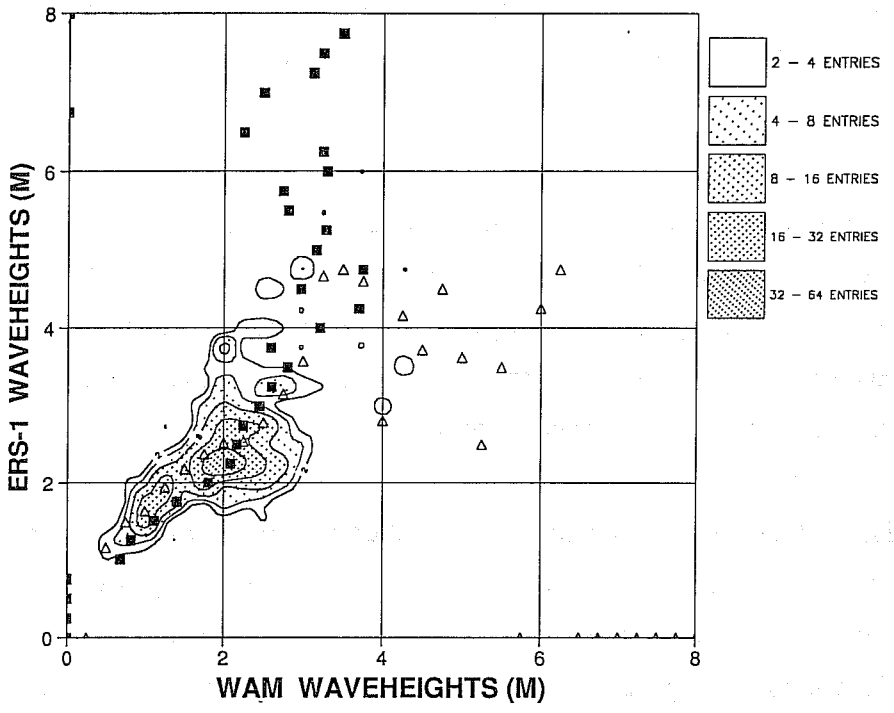

STATISTICS

ENTRIES	729
MEAN WAM	2.13
MEAN ERS–1	2.60
BIAS (ERS–1 – WAM)	0.48
STANDARD DEVIATION	0.80
SCATTER INDEX	0.38
CORRELATION	0.62
SYMMETRIC SLOPE	1.22

WAM–Model – ERS–1 – Comparison (ppt)
Radar – Altimeter – Windspeeds
period from 01/22/1992 16:06'37" to 01/23/1992 08:25'39"
GLOBAL

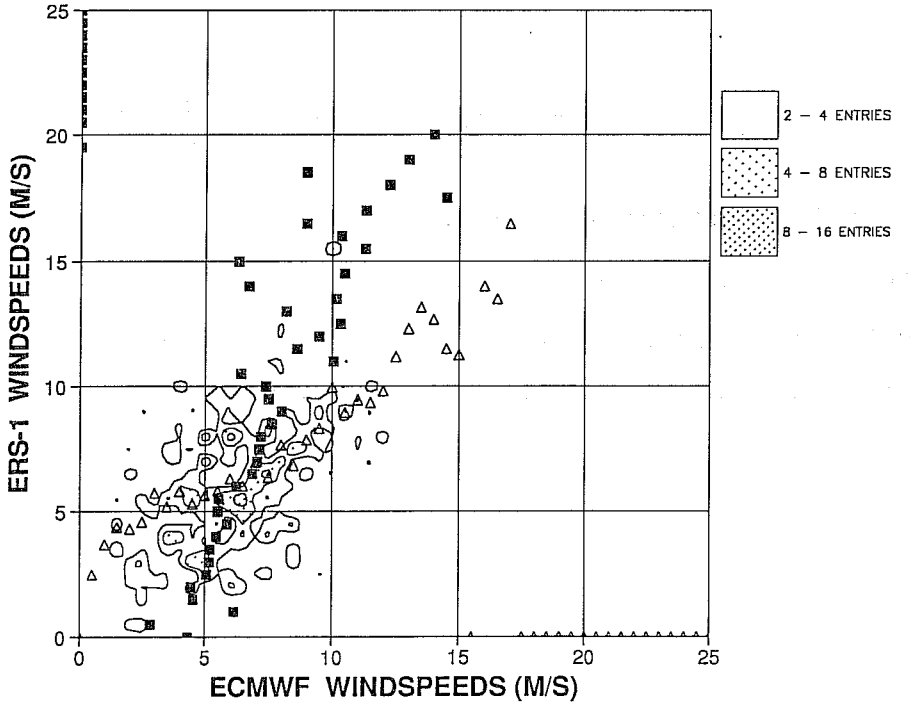

STATISTICS

ENTRIES	729
MEAN WAM	6.69
MEAN ERS–1	6.78
BIAS (ERS–1 – WAM)	0.09
STANDARD DEVIATION	3.30
SCATTER INDEX	0.49
CORRELATION	0.51
SYMMETRIC SLOPE	1.04

Fig 12 Day 8 statistics.

generated at a different location by an earlier forecasted wind field which is therefore presumably of better quality. Secondly, according to the energy balance (equation (12)), the wave spectrum is an integral over the input source function hence rapid changes and errors in the wind field will be averaged out, giving a reduced scatter. In other words, the wave height collocation diagram 12 looks so good because in the collocation we are mainly dealing with swell. On the other hand, the extreme states are not so well simulated as is evident from the mean WAM wave height as function of ERS-1 (■) or the mean ERS-1 wave height as function of WAM (Δ).

One may finally wonder whether these wind speed differences are associated with a (somewhat) different atmospheric circulation. For the day 4 forecast of 15 January 1992 they are as is illustrated in Fig 13 where we show the difference in 1000 mb and 500 mb geopotential height between coupled and control run. At the surface we note a typical dipole pattern with a maximum amplitude of 60 m (corresponding to about 8 mb in pressure) suggesting a shift in position of the depression which was present at that time.

Let us now return to the main issue of this section, namely why the differences in scores are so small between coupled and control run, while at the surface the differences in wind speed, eg, are rather significant. We conjecture that this is related to the fact that changes in the surface roughness over the oceans take such a long time to have impact on eg the pressure distribution. We estimate this time scale to be at least of the order of 5 days. In order to see this, we try to assess the impact of surface friction on the baroclinic instability or equivalently on the decay of a depression, without reverting to boundary layer schemes with complicated turbulent closure schemes. In the so-called quasi-geostrophic approximation (*Pedlosky*, 1987) one obtains for the mean vorticity equation in the absence of forcing

$$\frac{d}{dt}\zeta_o = -\frac{f}{D}w_o$$

where $\zeta_o = \frac{\partial}{\partial x}v_o - \frac{\partial}{\partial y}u_o$, where u_o and v_o are components of the geostrophic wind, $\frac{d}{dt}$ is the total derivative, f is the coriolis parameter, D the depth of the layer (or equivalent depth in case of atmospheric waves) and w_o is the vertical motion at the surface induced by the surface friction. The vertical velocity may now be related to the geostrophic wind in the following manner. First, we relate the vertical velocity to the curl of the surface stress by using the momentum balance close to the surface in the quasi-geostrophic approximation,

$$f(u-u_o) = \frac{\partial}{\partial z}(\tau_y/\rho)$$
$$-f(v-v_o) = \frac{\partial}{\partial z}(\tau_x/\rho)$$

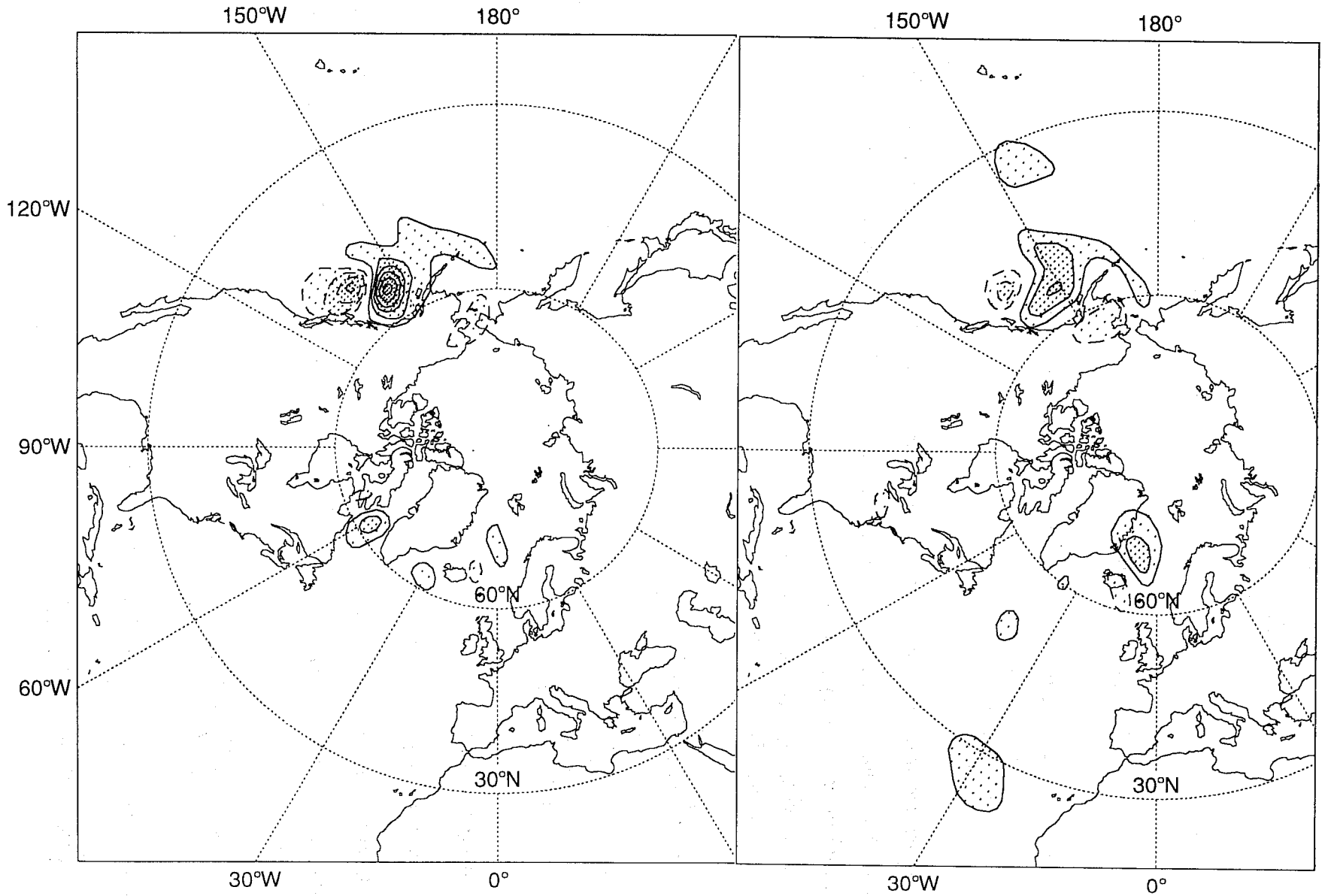

Fig 13 Differences in 1000 hPa and 500 hPa geopotential height between coupled and control run for day 4 forecast of January 15 1992.

where z refers to height and the geostrophic flow with components $u_o = -\partial P/\partial y/(\rho f)$, $v_o = \partial P/\partial x/(\rho f)$ is divergence free for a constant density (we take $\rho=1$). The horizontal divergence is then given by

$$\nabla\cdot\vec{u} = \frac{\partial}{\partial x}u + \frac{\partial}{\partial y}v = \frac{1}{f}\frac{\partial}{\partial z}\left\{\frac{\partial}{\partial x}\tau_y - \frac{\partial}{\partial y}\tau_x\right\},$$

and from the continuity equation we obtain the vertical component of the velocity

$$w = -\int_o^z \nabla\cdot\vec{u}\,dz = \frac{1}{f}\left\{\frac{\partial}{\partial y}\tau_x - \frac{\partial}{\partial x}\tau_y\right\}_o^z.$$

Since, by definition, there is no stress at the top of the boundary layer we have

$$w_o = -\frac{1}{f}\left(\frac{\partial}{\partial y}\tau_x - \frac{\partial}{\partial x}\tau_y\right)_{z=0}$$

The next step is to relate the surface stress with the geostrophic wind by means of an empirical geostrophic drag law. We use the one quoted by *Tennekes and Lumley* (1972). If α is the angle between the surface stress vector and the geostrophic wind, the drag law reads

$$\tau_x = \tfrac{1}{2}\, C_D\, U(u_o(1+\cos 2\alpha) - v_o \sin 2\alpha)$$
$$\tau_y = \tfrac{1}{2}\, C_D\, U(u_o \sin 2\alpha + (1+\cos 2\alpha)v_o)$$

where $U = \sqrt{u_o^2+v_o^2}$ and the drag coefficient C_D is

$$C_D = \left\{\frac{\kappa}{\left[\ln\left(\frac{u_*}{fz_o}\right) - \kappa C\right]}\right\}^2,$$

while the angle α is given as

$$\tan\alpha = A\, C_D^{1/2}$$

where the empirical coefficients A and C have values $A = 12$, $C = 4$ and z_o is the surface roughness. It is now straightforward to obtain the curl of the surface stress field with the following result for the vertical velocity

$$w_o = \frac{1}{f}\,\frac{C_D U}{(1+A^2 C_D)}\left[\frac{\partial}{\partial x}v_o - \frac{\partial}{\partial y}u_o\right]$$

and therefore the decay law for the large scale vorticity becomes

$$\frac{\partial}{\partial t}\zeta_o = -\gamma\,\zeta_o,\ \gamma = \frac{C_D U}{D(1+A^2 C_D)} \qquad (16)$$

It should be pointed out that the damping rate thus obtained is in marked contrast to the textbook result found with a constant eddy viscosity A_v. From eg *Pedlosky* (1987) one has

$$\gamma = (A_v f/2)^{1/2}/D$$

which shows a much more sensitive dependence on the coriolis parameter. The constant eddy viscosity model is, however, rather unrealistic because the angle between geostrophic wind and surface wind is always 45° which is in contrast to field observations which give angles in the order of 20°.

We are now in a position to estimate some decay time scales over young wind sea, old wind sea and land. They are displayed in Table 2. We took as equivalent depth D = 5 km, the geostrophic wind was taken as a constant and, over sea, we took the Charnock relation for the roughness.

U = 15 m/s		
	α	γ (days^{-1})
old sea ($z_o = \alpha\, u_*^2/g$)	0.0185	0.18
young sea ($z_o = \alpha\, u_*^2/g$)	0.0925	0.23
land (z_o = 10 cm)	-	0.39
U = 25 m/s		
	α	γ (days^{-1})
old sea	0.0185	0.32
young sea	0.0925	0.40
land	-	0.60

Table 2: Damping rates for different wind speeds and sea states. Here D = 5 km, A = 12, C = 4.

We observe from Table 2 a modest sensitivity of damping rates on the sea state. How do these damping rates compare with the growth rates obtained from the baroclinic instability in the absence of dissipation. See for this Fig 14 which is from *Valdes and Hoskins*, 1987 who calculated growth rates from the mean Northern Hemisphere winter climate.

Clearly, damping rates are of the same order of magnitude as the growth rates, thus the effect of surface friction on the baroclinic instability may be relevant. This suggests that for the mean winter climate with U = 15 m/s different sea states may give rise to differences in the total growth rate of about 25% so that

significant differences in amplitude only occur over the long time scale of about 5 days. Because of this long time scale it should be noted that this picture may be obscured by nonlinear wave-wave interactions and effects of wave-mean flow interaction.

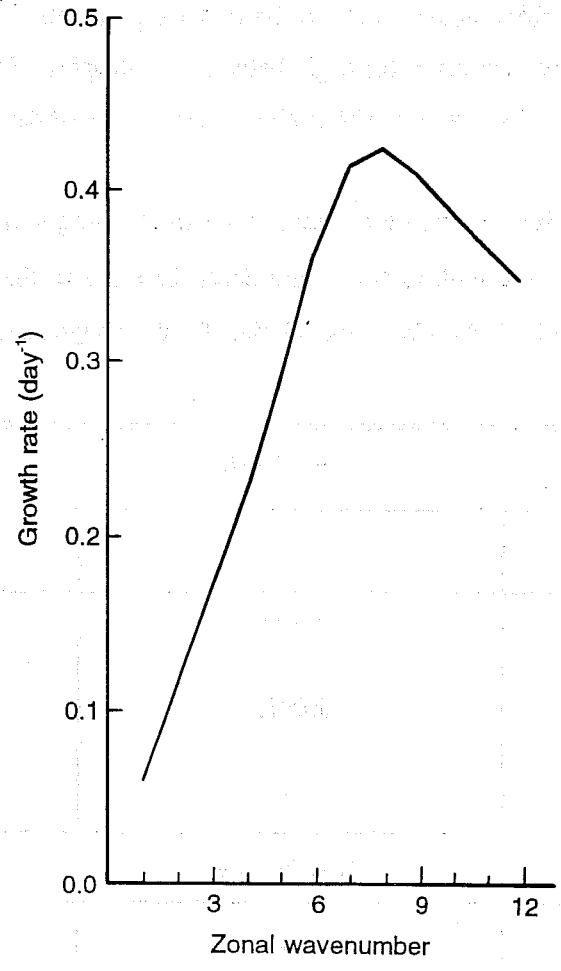

Fig 14 Growth rate of baroclinic instability for Northern Hemisphere winter climate. Full line: no dissipation.

Finally, it should be pointed out that there may be another reason why the impact of increased roughness on the pressure field is so small. Returning to the momentum balance near the surface and applying it to the surface one would obtain

$$\nabla^2 p = \nabla \cdot \frac{\partial}{\partial z} \tau \tag{17}$$

and therefore the surface pressure is an integral of the vertical gradient of the surface stress. Hence, random changes in the surface stress are averaged out so that only systematic changes in stress may contribute to a change in surface pressure. Traditionally, these systematic changes in surface stress are expected to be small. It is therefore concluded that only systematic changes in surface stress will contribute to a change in pressure distribution. Of course, it remains to be seen whether the systematic change in surface stress is sufficiently large to induce a significant impact on the atmosphere circulation.

We conclude from this lengthy discussion on the time scale for impact that, in order to see more impact of two-way interaction, we have to meet one of the following conditions:

(i) Guarantee that the initial condition is in agreement with the coupled model physics. This means analysis experiments with the coupled model have to be performed.

(ii) Under extreme conditions the effect of two-way interaction is, according to Table II, more pronounced.

(iii) Perform climate runs to investigate any systematic impact on atmospheric circulation.

Item (i) will be addressed in the second part of this project, while forecasts of extreme events will be discussed next. Results of 90 day climate runs will be studied in the next section.

We selected extreme events by inspection of the archived WAM model plots over the year 1991. Under the header 'Analysis' we have listed the extreme events which we selected for our next set of runs. We have also given the ocean in which the extreme event occurred.

The date in the table refers to the start date of the forecast. As a rule, in order to obtain a balance between the atmospheric state and the coupled physics, the extreme event took place 2 days after the start date of the forecast.

START DATE	OCEAN	ANALYSIS Hmax(m)	2D FOREC(cy44) Hmax(m)	2D FOREC(cy36) Hmax(m)
910110	NATL	17	12	17
910130	NATL	14	9	11
910220	NPAC	13	9	10
910227	NATL	16	12	17
910314	NPAC	15	11	14
910331	NPAC	15	9	12
910304	SH	17	13	17
910606	SH	15	9	14

Table 3: List of extreme events during 1991.

We performed the usual 10 day forecasts with our coupled code in one and two-way interaction mode and we found, much to our surprise, that the extreme waves were underestimated to a considerable extent. Results from the control run at day 2 are listed under the header 2D FOREC(cy44) and show a mean difference of about 5 m in wave height. In order to check whether there was a problem with forecasted winds, and at the same time checking the analysis from 1991, we reran the WAM model with archived forecast winds from the then operational model cycle 36. The results are displayed in the last column of Table 3, and although there are differences, the maximum wave height is only underestimated by 1 m on average. To illustrate how big the differences are, we show in Fig 15 the wave height field from the winds from cy44 and cy36 for the forecast with start date 910227.

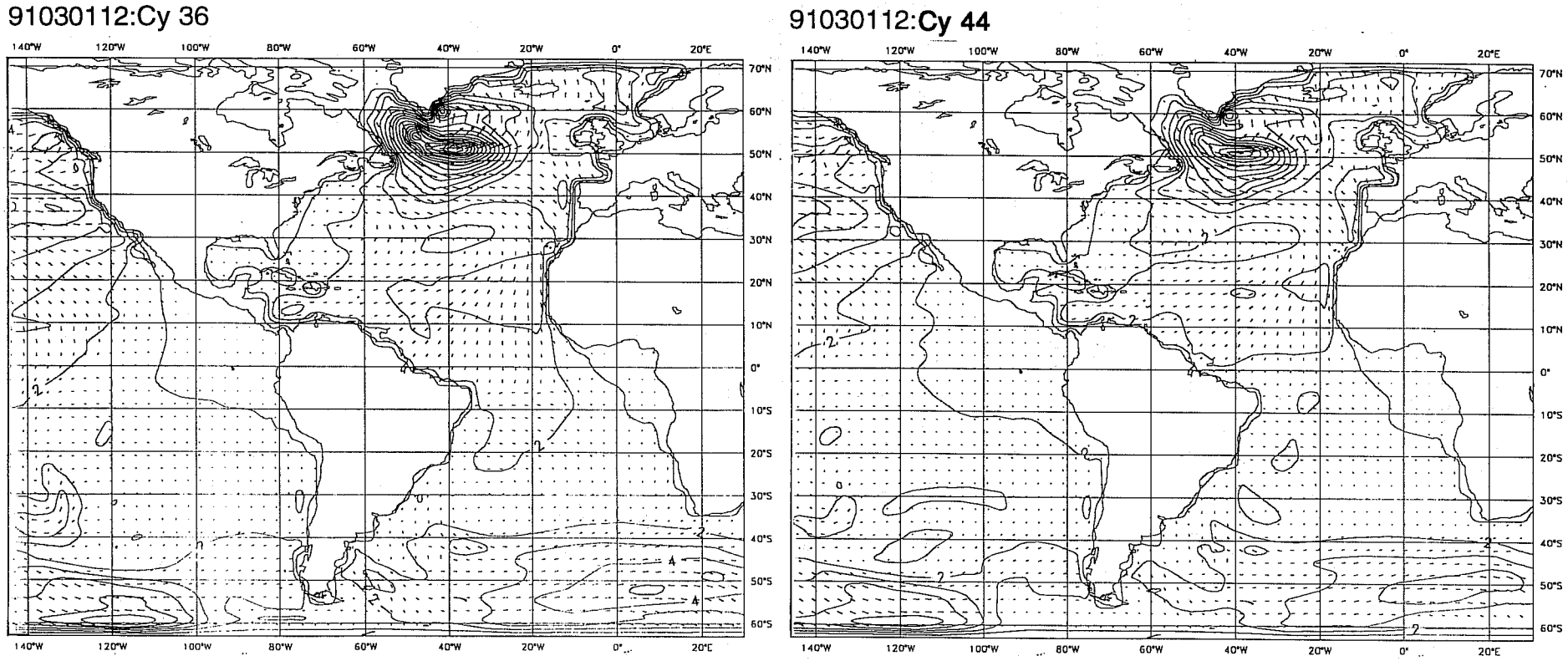

Fig 15 2D wave forecast from winds of cy36 and cy44.

Evidently, these differences arise because of the different wind fields produced by the cy36 and cy44 versions of the ECMWF model, but it is not easy to give a reason for the reduction in wind speed because there are many physical and dynamical differences between cy36 and cy44. The most likely reason is, however, the change in integration scheme from a time split scheme to a fully implicit scheme. *Janssen et al* (1992) discovered an inconsistency between wind speed and surface stress when using the time split scheme. The result was that the drag coefficient was too low for high wind speed. This inconsistency was removed when a fully implicit scheme was used. Since to first approximation the surface stress is determined by the pressure gradient (cf Eq (17)), the consequence was that wind speeds were reduced, especially in the high wind speed range.

This explains, to some extent, the reduction in wind speed as it is produced by the present cycles of the ECMWF model. The question now is which cycle is producing the right winds. This question is not easy to answer because extreme events usually occur where there are hardly any conventional (eg ship) data. Presently, there is evidence (*Komen et al*, 1993), however, that the newer cycles of the ECMWF model are producing too low wind speed in the high wind speed range. This follows from comparison of operational WAM results with altimeter and SAR data.

The question then finally is how to increase wind speeds in the present cycles of the ECMWF model. Returning to the time split scheme does not seem to be a good idea because consistency between surface stress and surface wind would be lost. It seems more likely that, in extreme events, the surface stress is too low which implies that, in these circumstances, the pressure gradient is too low (although from a comparison with observations Stoffelen could find no evidence for errors in the pressure field). This suggests that either the resolution of the numerical model is too low (which is not unlikely because gradients might become very large) or that there is too much smoothing caused by eg numerical diffusion. Alternatively, noting that these severe storms were associated with cold air outbreaks giving a gusty wind, inclusion of gustiness may also resolve, to some extent, the problem since it gives rise to a more rapid growth of the long waves. A list of related problems in the planetary boundary layer has been reported by *Hollingsworth* (1994).

With these reservations in mind, in Fig 16 we now present the anomaly correlation of 500 mb height for the North Pacific and North America. We took the mean over 6 cases and evidently now a small beneficial impact (both over the Pacific and North America) for the coupled run is observed. In agreement with our previous remarks, the time scale for impact to occur is about 5 days and we cannot escape the impression that another reason why we have impact here is that, at day 5 in the forecast, the quality of the forecast is still so high.

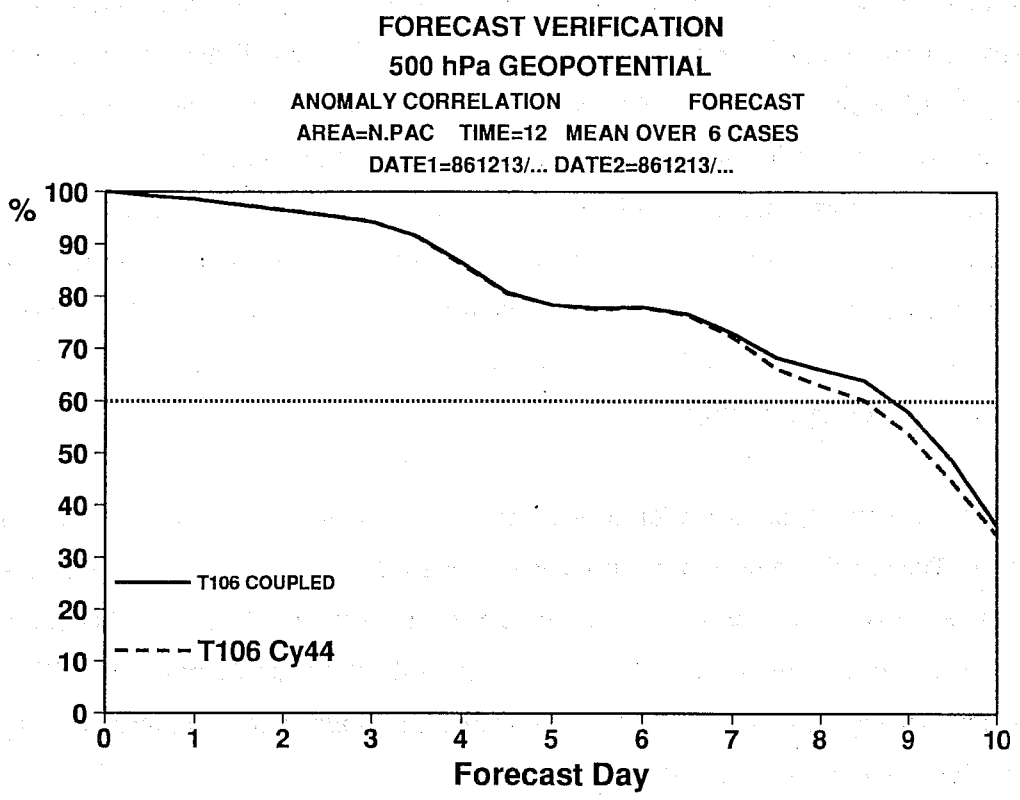

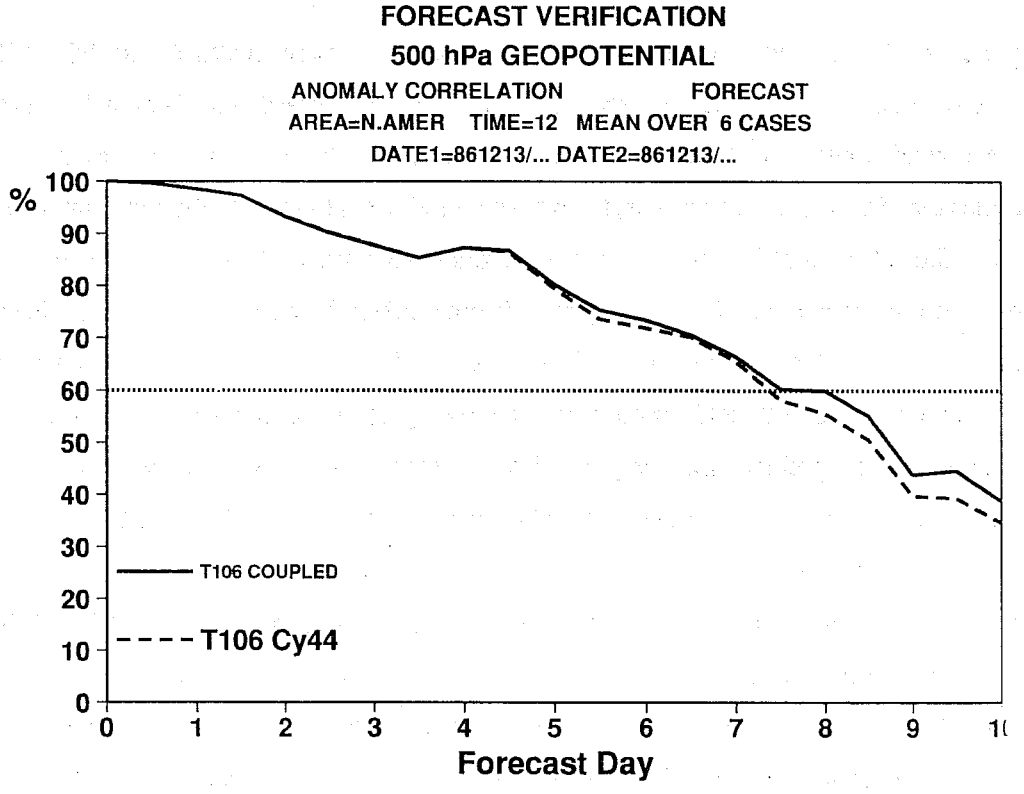

Fig 16 Anomaly correlation of 500 mb geopotential height field over North Pacific and North American continent.

3.4 Seasonal forecasts

As the time scale for impact to occur is quite long, one would expect more substantial impact with climate runs. To that end we performed a number of 120 day runs with the T63 version of the coupled model and compared the mean over the last 90 days with results from the model with one-way interaction only. When comparing results of one run, substantial differences in wave field, surface stress, geopotential height, temperature and rainfall are found. The important question to ask now is whether these differences are due to changes in the physical formulation between coupled and control run or due to the sensitive dependence of the atmospheric model to changes in the initial condition (Butterfly effect). To appreciate this point we will show the mean difference in stress for the run that started the next day and, in fact, a difference picture will be found that is completely different from the previous one. Thus, in order to obtain reliable information on the impact of waves on the atmospheric circulation, there is need for Monte Carlo forecasting. This approach is, by the way, well-known in climate modelling studies (see eg *Ferranti et al*, 1993). We therefore performed five coupled and control runs for the winter season of 1990 and the summer season of 1989 starting from 5 consecutive days, thus providing a more reliable estimate of the mean state of the atmosphere at a certain location. At the same time we may infer from the scatter around the mean information on the variability, thus a t-student test may be applied to test the statistical significance of the mean difference between coupled and control run. Results are found to be statistically significant indeed, so that it is shown that two-way interaction has a definite impact on atmospheric circulation.

Let us first discuss some details of a single run for the winter season 1990 and the summer of 1989. Both seasons had hardly any El Niño/La Niña activity so they may be regarded as typical. First, the winter of 1990.

The starting date of the 'typical' 1990 winter run was 1 November 1990. We will only show 90 day means starting from 1 December, 1990. The wave height and friction velocity field of the coupled and control experiment and the differences are shown in Fig 17 and Fig 18 respectively. Differences are rather big.

Considering the mean wave height fields and their differences, it is evident that in the coupled run there is a considerable shift in the North Atlantic storm track towards the south, while the region of maximum activity in the North Pacific is shifted to the east and the mean wave direction is more westerly. In the Southern Hemisphere the regions of maximum activity in the Indian Ocean and the Southern Atlantic are shifted towards the equator, suggesting that, in the coupled run, the flow is less zonal. These features are also evident in the mean friction velocity field. In addition, the increase in friction in the trade wind area in the Pacific should be noted.

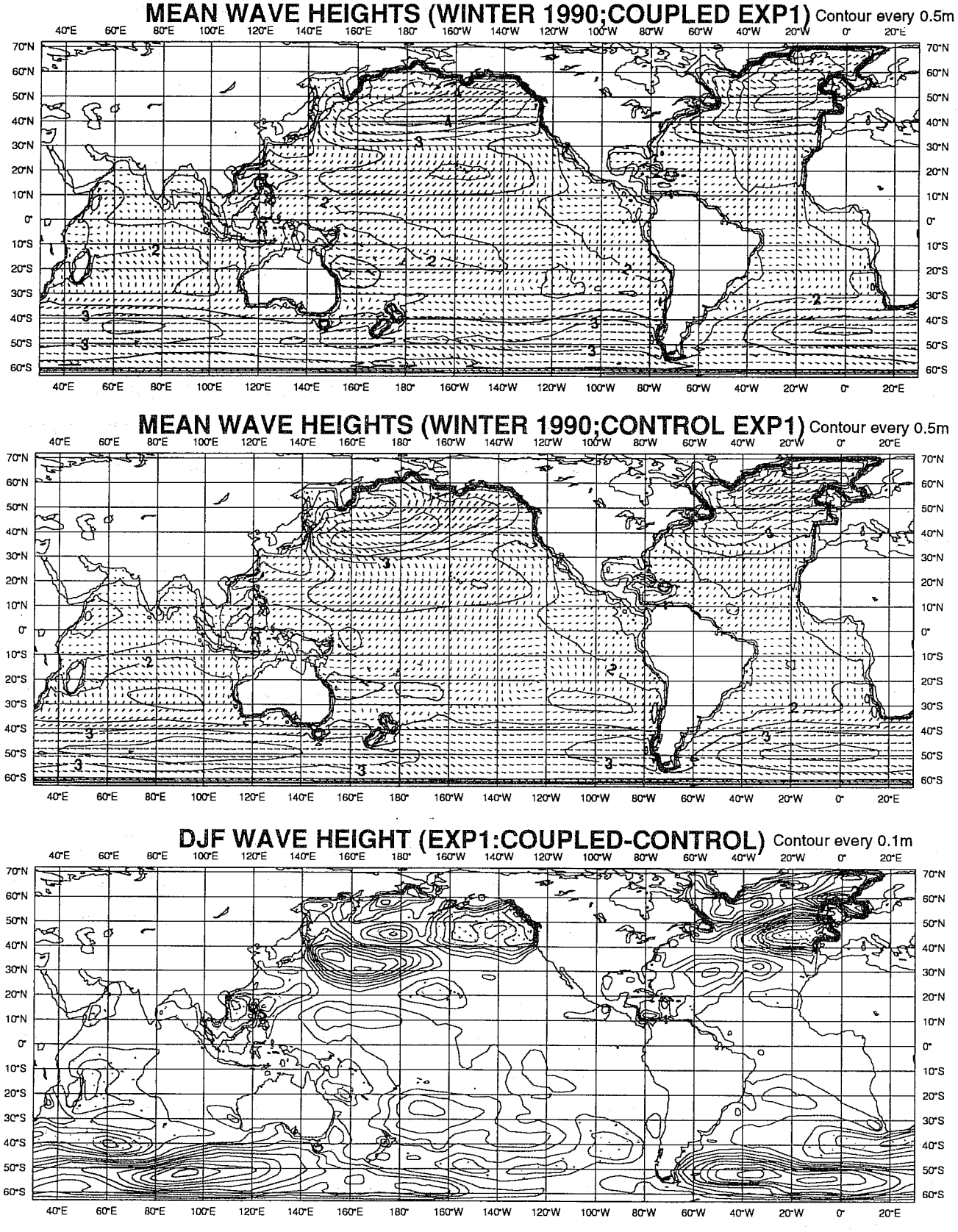

Fig 17 90 day mean of wave height for coupled and control experiment. Also differences are shown. Positive differences are denoted by dotted shading.

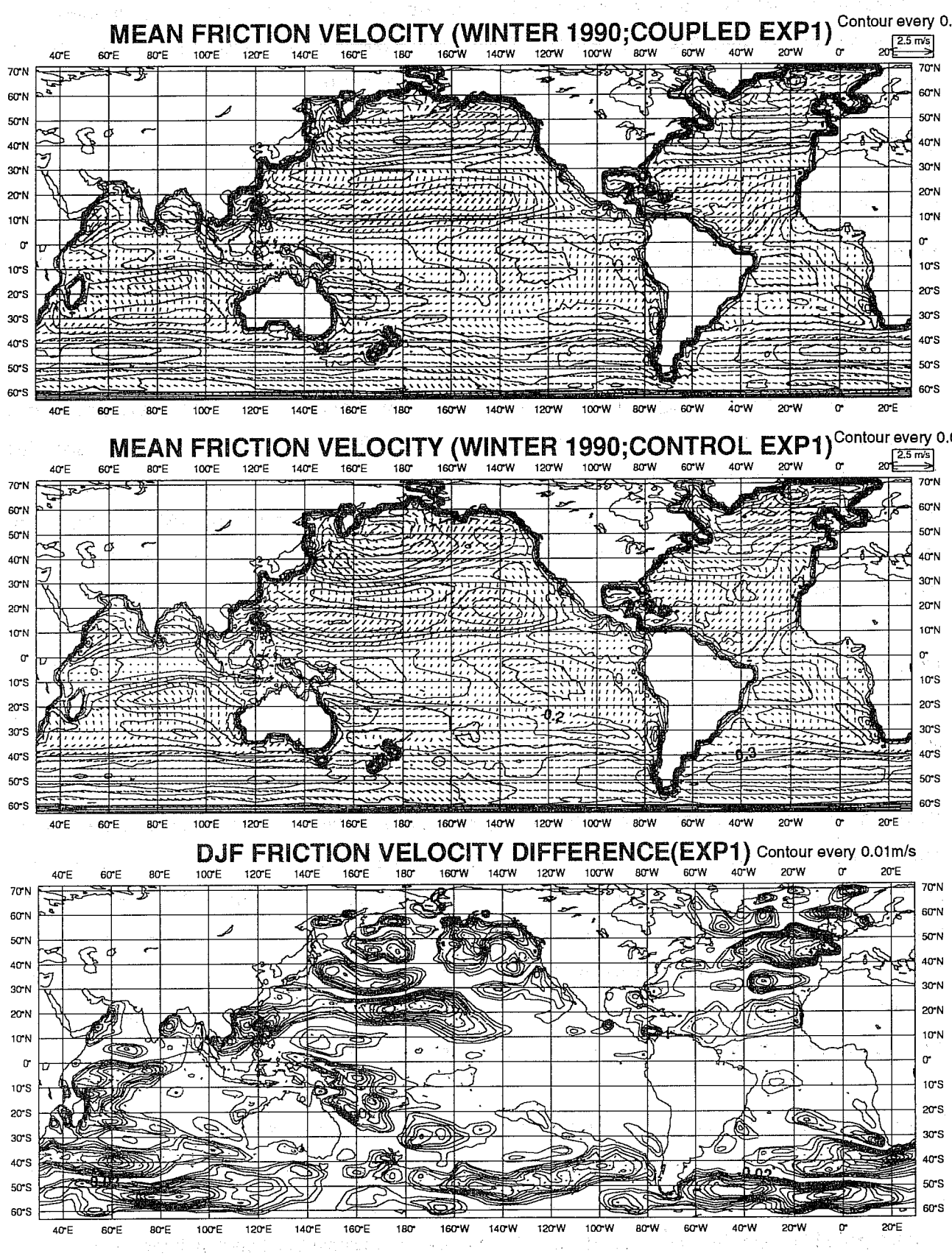

Fig 18 90 day mean friction velocity for coupled and control experiment. Also differences are shown, where positive differences are indicated by dotted shading.

Although there may be considerable regional differences in wave height, friction velocity and wind speed, (not shown) it should be pointed out that there is hardly any difference in the wind and wave statistics of coupled and control run. The wave height and wind speed distribution, shown in Fig 19, are virtually identical which is supported by the mean statistics presented in Table 4.

	$<H_s>$(m)	$<U_{31}>$(m/s)	s.d. H_s(m)	s.d. U_{31} (m/s)
coupled	2.35	7.93	1.00	3.84
control	2.43	7.96	1.06	3.91

Table 4: Mean and standard deviation of wave height and wind speed distribution for coupled and control run.

Let us now discuss some differences in the meteorological fields. In Figs 20a, b and c we show the 500 and 1000 mb geopotential height field and the 850 mb temperature field for coupled and control run. Differences are quite large, eg the maximum difference in the 500 mb height field is 200 m corresponding to 25 mb in pressure, and they have a large spatial scale. Also note the warming up over the continents, especially the North American continent. The flow pattern at 500 mb is consistent with our observation from the surface friction field that there is a shift in the storm track towards the equator. This shift in storm track may have important consequences for other meteorological parameters.

Consider eg the mean rainfall which is displayed in Fig 21. In the coupled run, owing to the shift in storm track, there is an intensification of rainfall over Western Europe and the west-coast of North America. This suggests that the atmosphere over these continents is more moist which seems consistent with the increase in 850 mb temperature noted before. We also note some changes in the rainfall pattern over the Indian Ocean and Africa. The change in pattern over the Indian Ocean may be related to the increase of drag coefficient by some 20% in the low wind speed range (cf Fig 9). Finally, in Fig 22 we show the mean latent heat flux over the globe. There are considerable changes related to the shift in the storm track to be noted, while we also observe some impact due to the waves on the latent heat flux distribution over the Indian Ocean, Africa and the Southern Pacific. We recall that the choice of the linear dependence of heat and moisture exchange on the drag coefficient is probably not correct. Therefore, the presently found dependence of the latent heat flux on the sea state may be an exaggeration.

This concludes our discussion of the winter 1990 run. Evidently, we have seen a considerable impact of two-way interaction on the atmospheric circulation and fluxes. Similar differences may be noted regarding the summer 1989 run, but we will not go into too much detail. In Fig 23 we only show the mean rainfall over the period between June and August, with the objective to illustrate that two-way interaction does not upset the tropical circulation pattern. On the contrary, a hole in the rainfall pattern above Indonesia, which is observed in the control run (and which should not be there), is removed when two-way interaction is

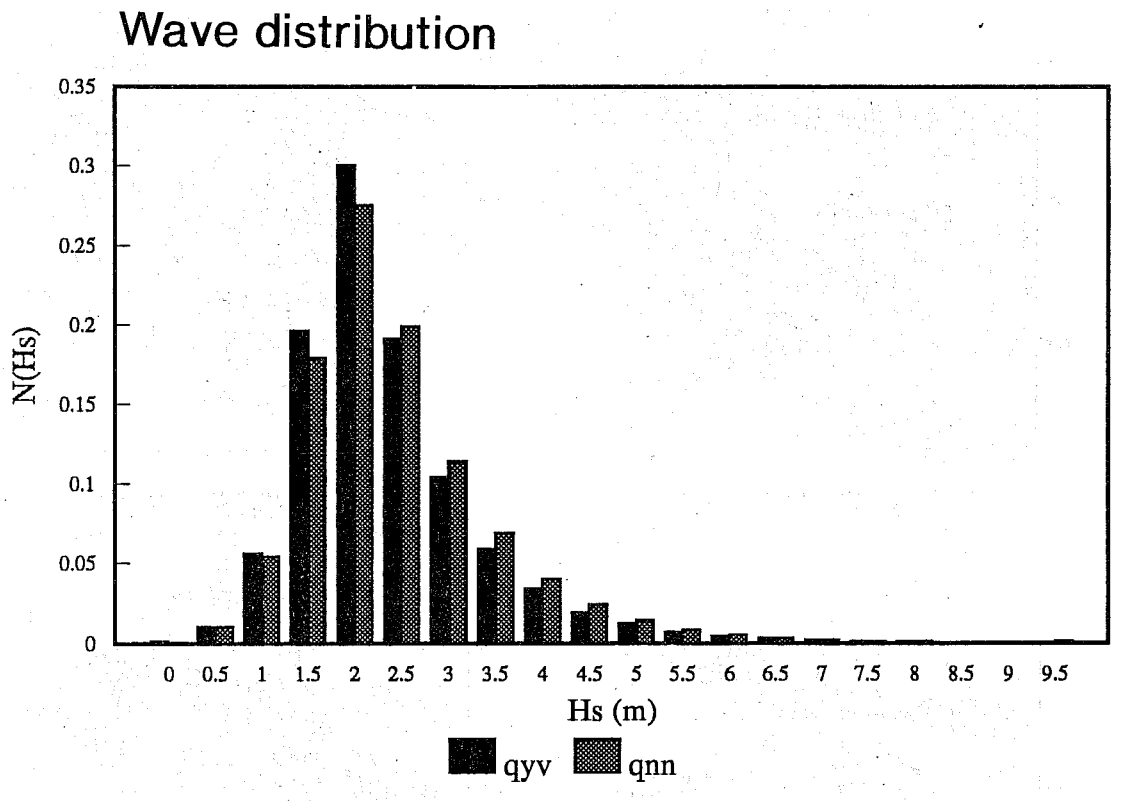

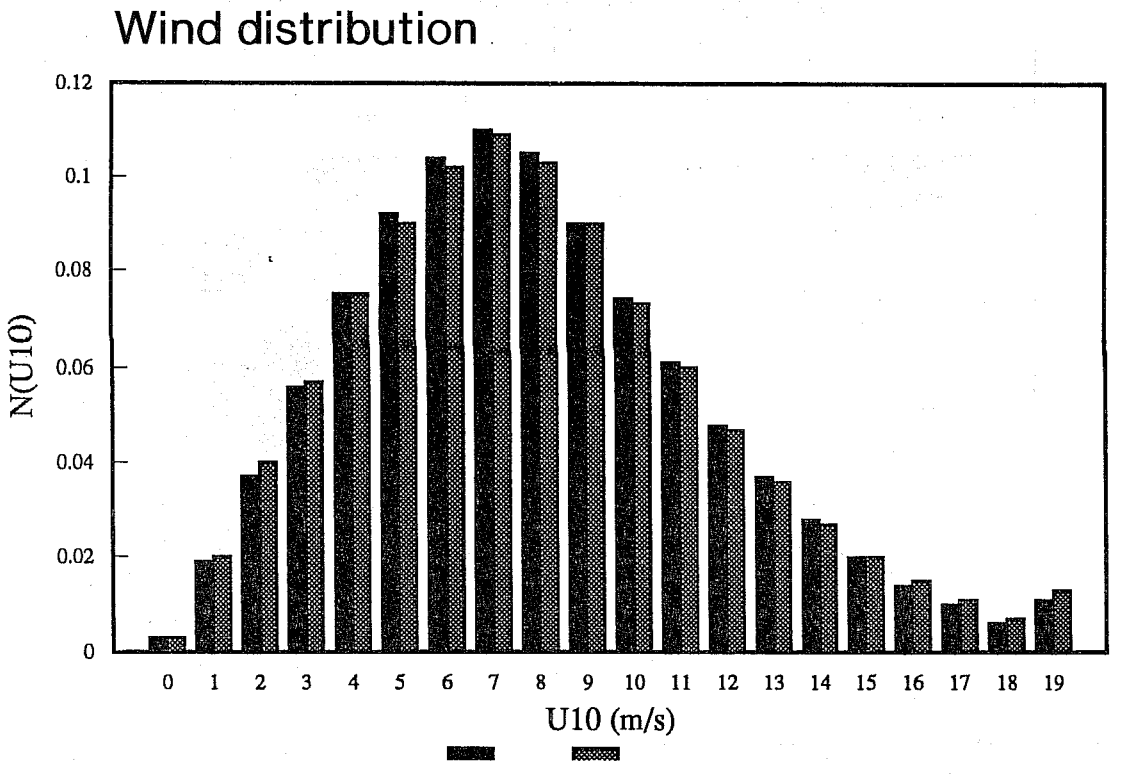

Fig 19 90 day average of wind and wave distribution.

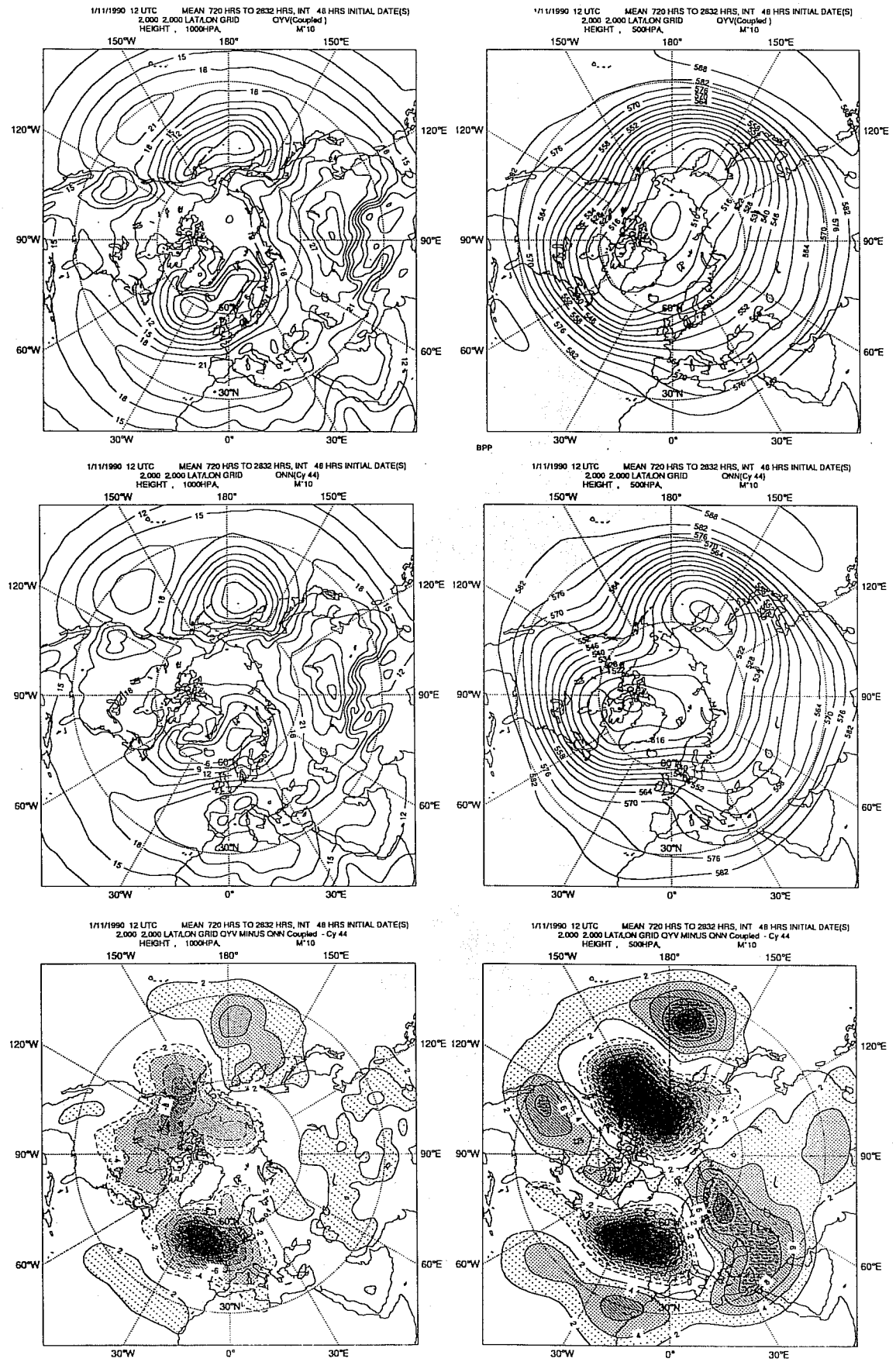

Fig 20a and b 90 day mean of 1000 mb and 500 mb height field for coupled and control run. Lower panel shows the differences.

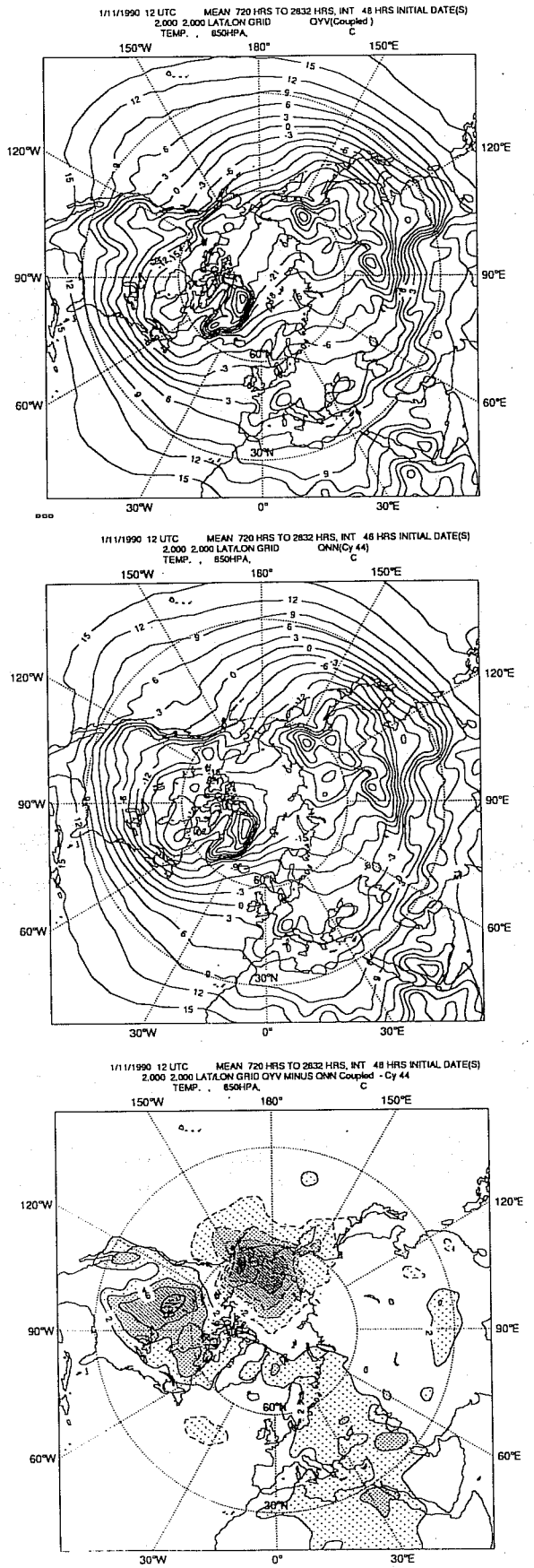

Fig 20c 90 day mean of 850 mb temperature field for coupled and control run. The lower panel shows the mean of the temperature difference.

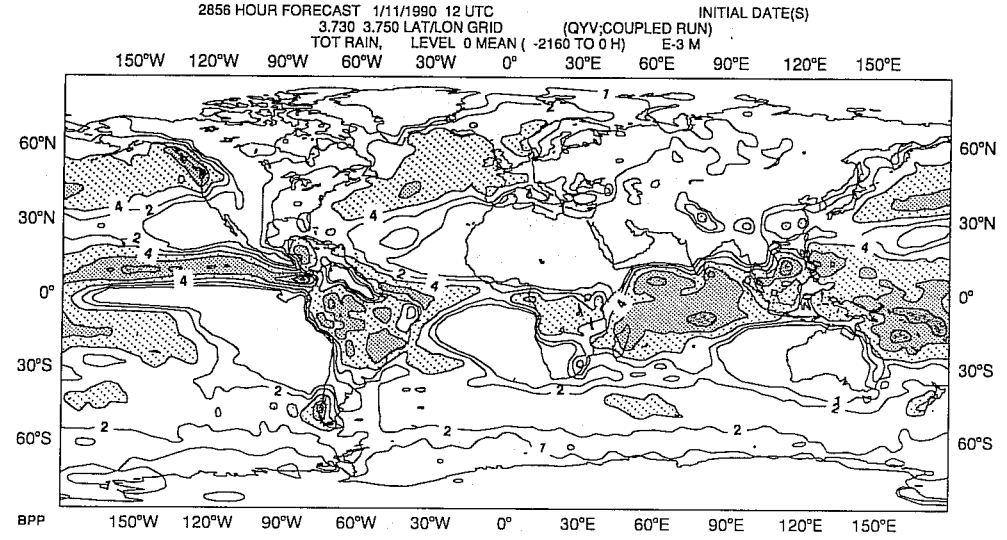

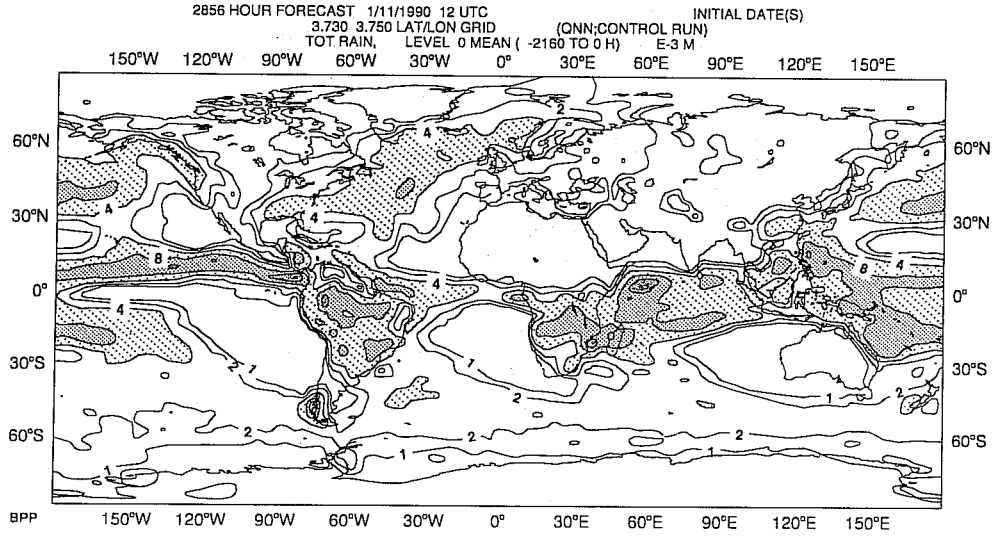

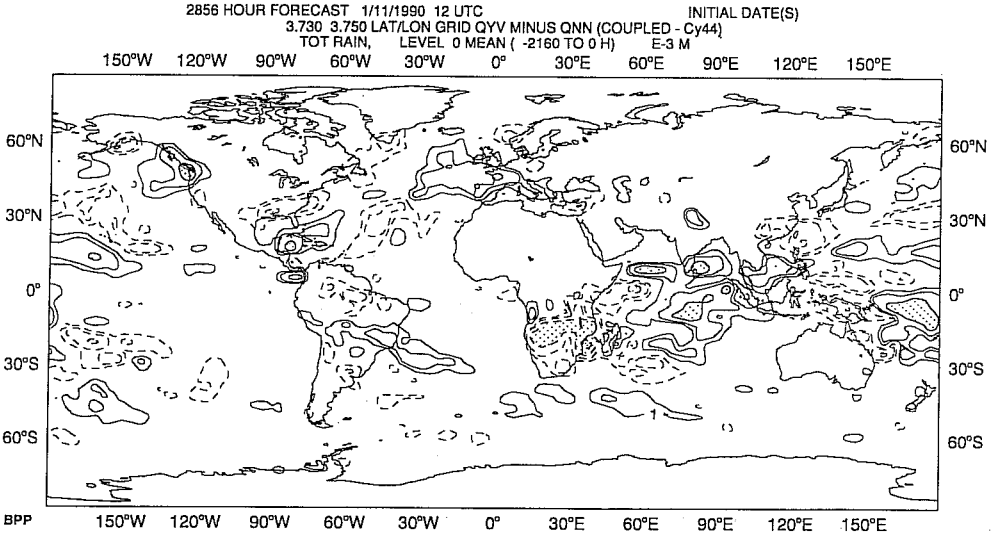

Fig 21 Mean rainfall and difference.

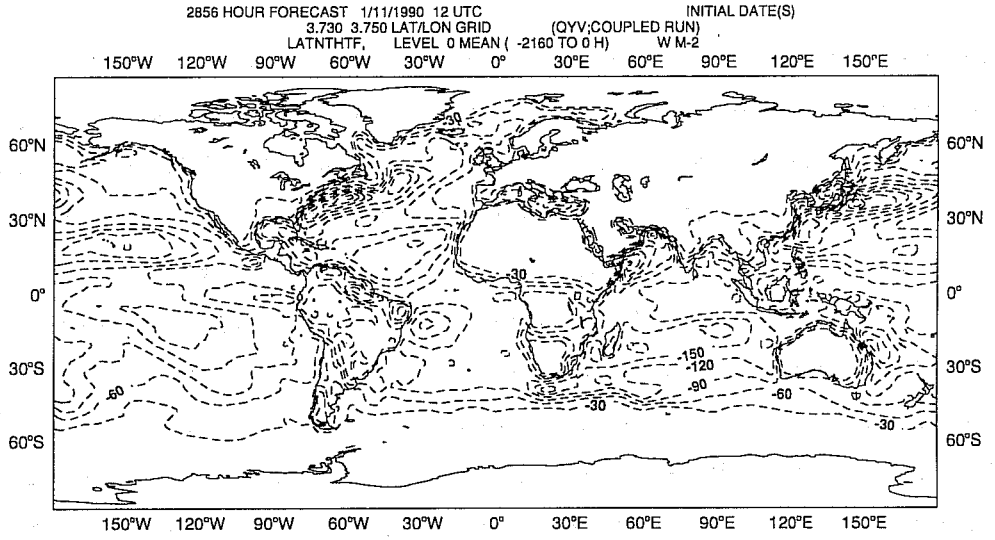

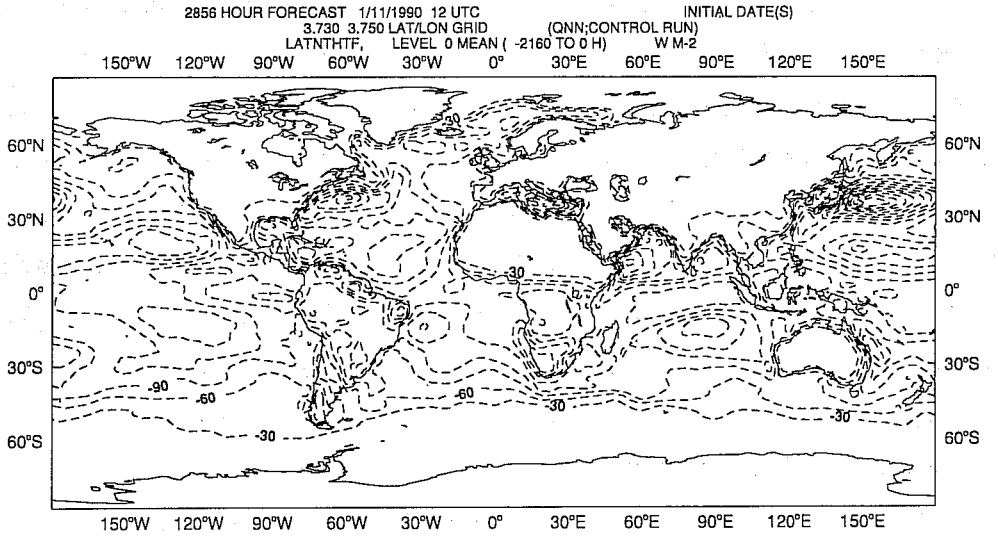

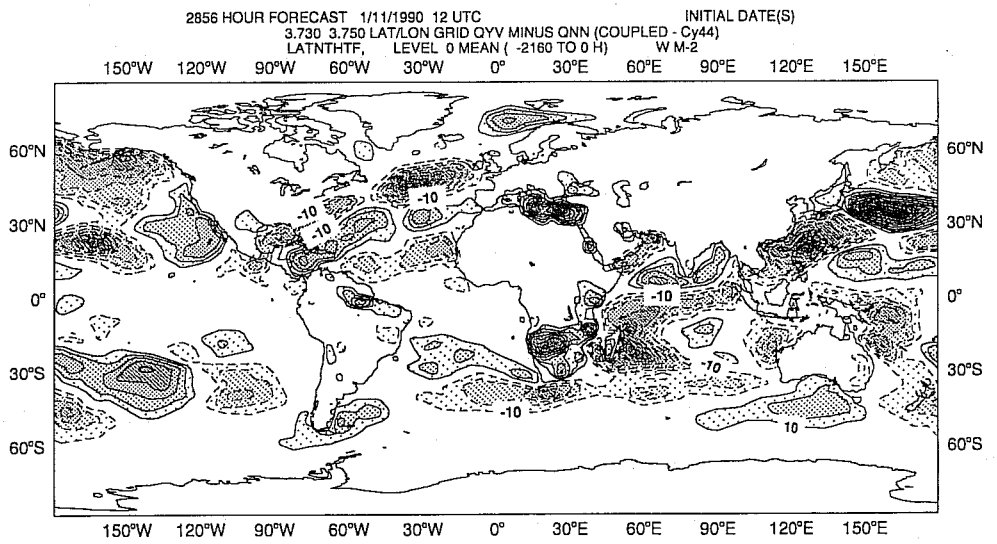

Fig 22 Mean latent heat flux and difference.

switched on. This change in rainfall pattern may be related to an intensification and shift of the monsoon over the Arabic Sea and the Indian Ocean, as may be observed from the mean friction velocity difference displayed in Fig 24.

We conclude that a comparison of results from individual experiments with the two- and one-way interaction codes shows considerable differences in wave height, friction velocity, rainfall, heat flux and geopotential height. It is important to wonder whether these differences are due to a different formulation of the momentum transfer or due to a sensitive dependence of the atmospheric model to change in the initial condition. In order to test the dependence on the initial state, we redid the winter run of 1990 but now took 2 November 1990 as initial date instead of 1 November 1990. The resulting mean difference of friction velocity between coupled and control run is shown in Fig 25 and, for comparison, we also show the mean difference from the run starting 1 November 1990, which was already displayed in Fig 18. What is so striking about this comparison is that these difference plots look so dissimilar. For example, in the second experiment, the intensification of the trade winds in the North Pacific has disappeared, the storm track in the North Atlantic has shifted to the North instead of the South and also patterns in the Southern Ocean look different. It is therefore clear that there is a dependence of the differences in meteorological quantities on the initial conditions. In order to distinguish the impact of the initial conditions from the impact of the ocean waves on the mean atmospheric circulation, one has to perform simulations from a large variety of initial conditions and the effect of the initial conditions is then removed by considering the ensemble mean state. In other words, one needs to perform Monte Carlo forecasting, an approach which is well-known in climate modelling studies (see eg *Ferranti et al*, 1993). We therefore performed five coupled and five control runs starting from 5 consecutive initial dates for the winter season of 1990 and the summer season of 1989, thus giving a more reliable estimate of the mean state of the atmosphere by means of ensemble averaging. At the same time, the statistical significance of the mean difference between coupled and control run could be tested by means of the t-student test because the variability around the mean at a certain location is known. This variability is inferred from the scatter around the ensemble mean produced by the individual realisations of the ensemble and is thus a measure for the long term (90 day) variability of the atmosphere.

In Figs 26-28 we show the ensemble mean of wave height, 31 m wind speed and friction velocity of the coupled and control run and their differences for the winter season of 1990. Comparing the differences with the results from a single run (cf Figs 17 and 18) it is clear that the amplitude of the differences is now much reduced, but several features are still noticeable. The storm track in the Southern Hemisphere is shifted towards the equator and there is some evidence that the storm track in the Northern Pacific is shifted to the South. However, there is no evidence of a shift in the storm track in the Northern Atlantic, except that winds get reduced by about 0.75 m/s north of 50° N and that east of the North American east coast the sea

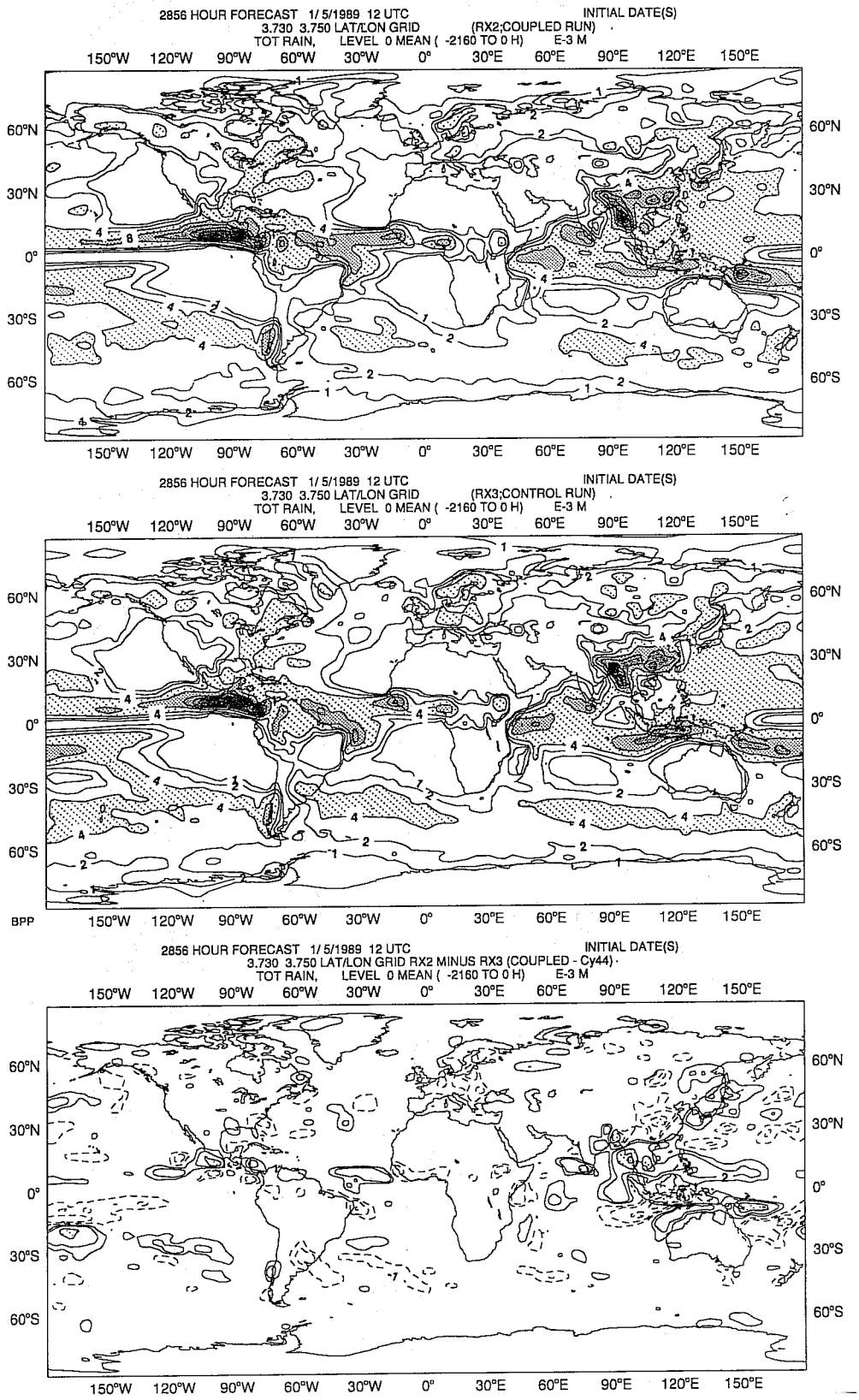

Fig 23 Mean rainfall and differences in summer 1989.

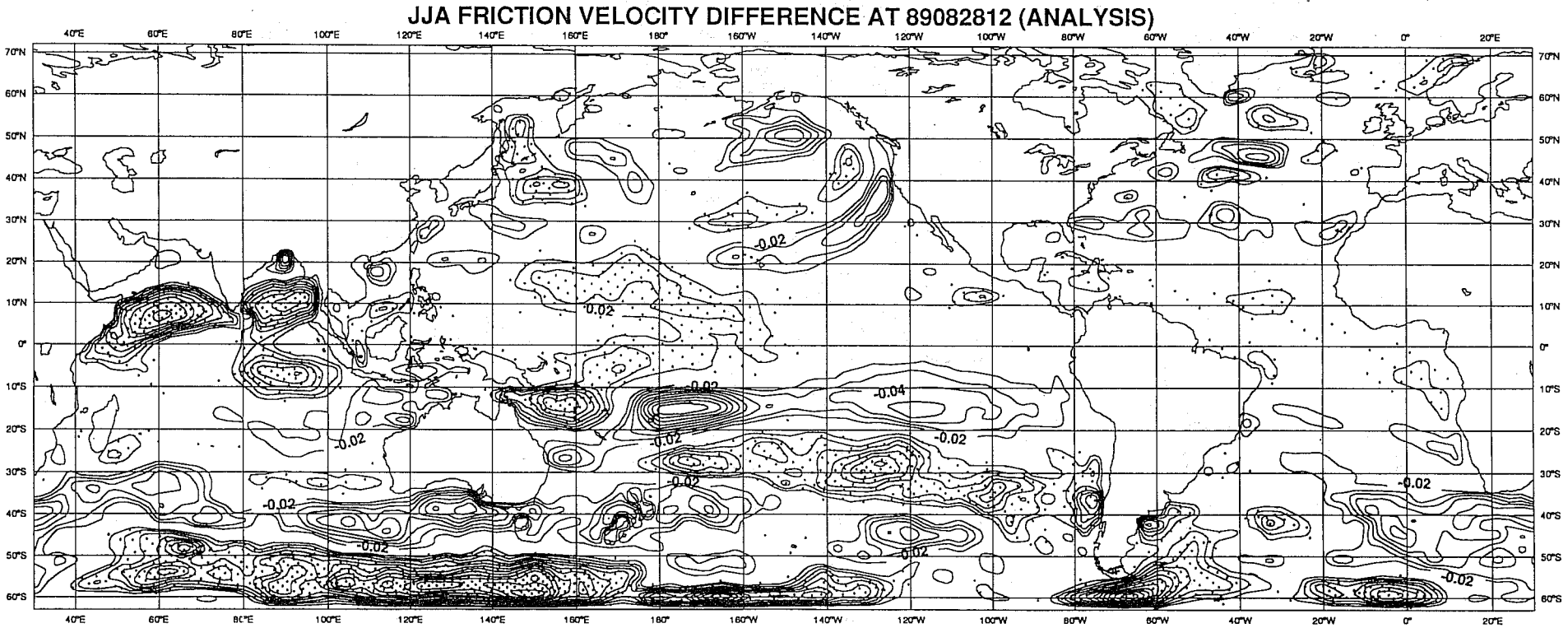

Fig 24 Mean friction velocity difference in summer 1989.

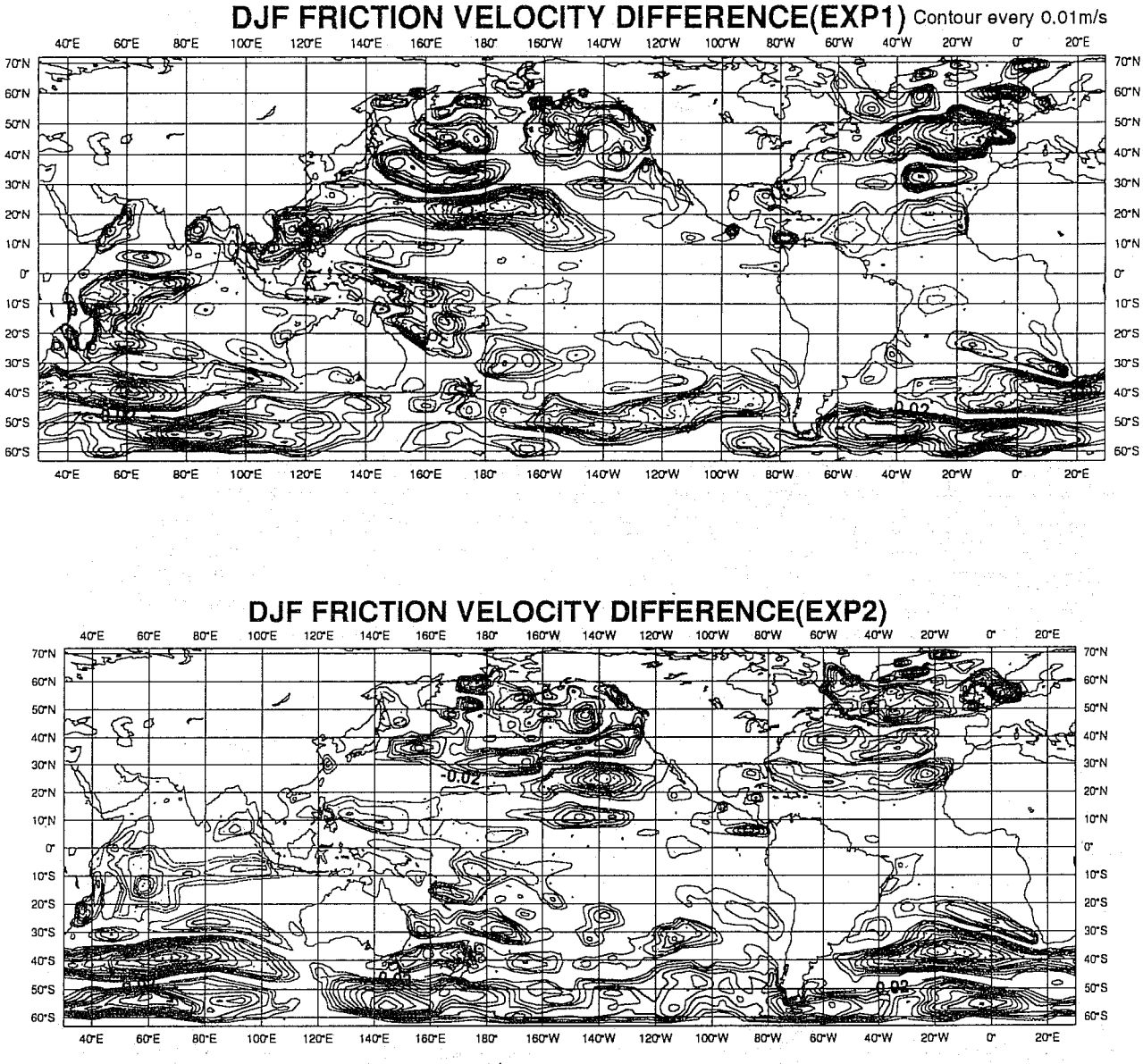

Fig 25 Comparison of two friction velocity difference plots starting from 1 November 1990 (top) and 2 November 1990 (bottom).

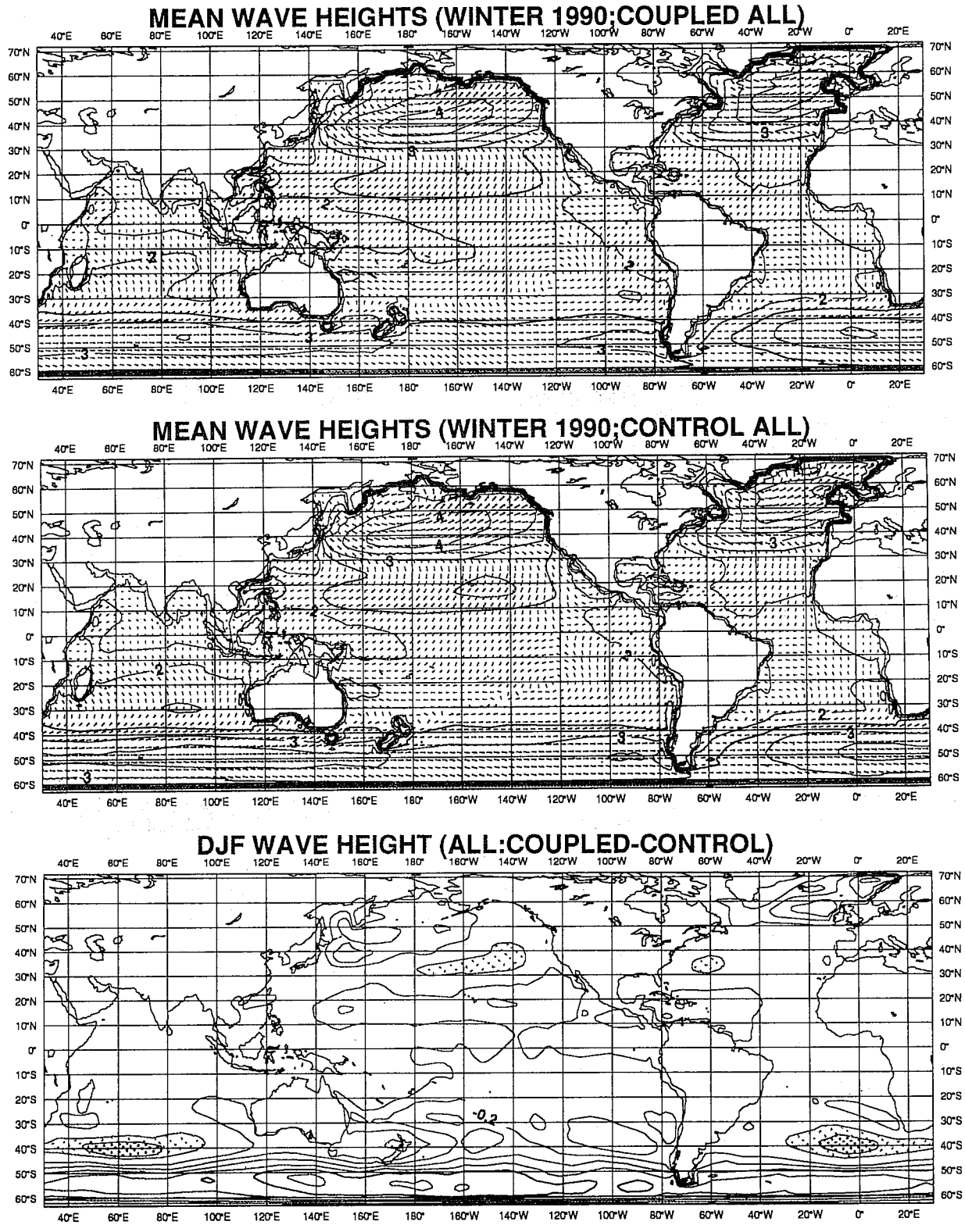

Fig 26 Ensemble mean of wave height for coupled and control run and the difference.

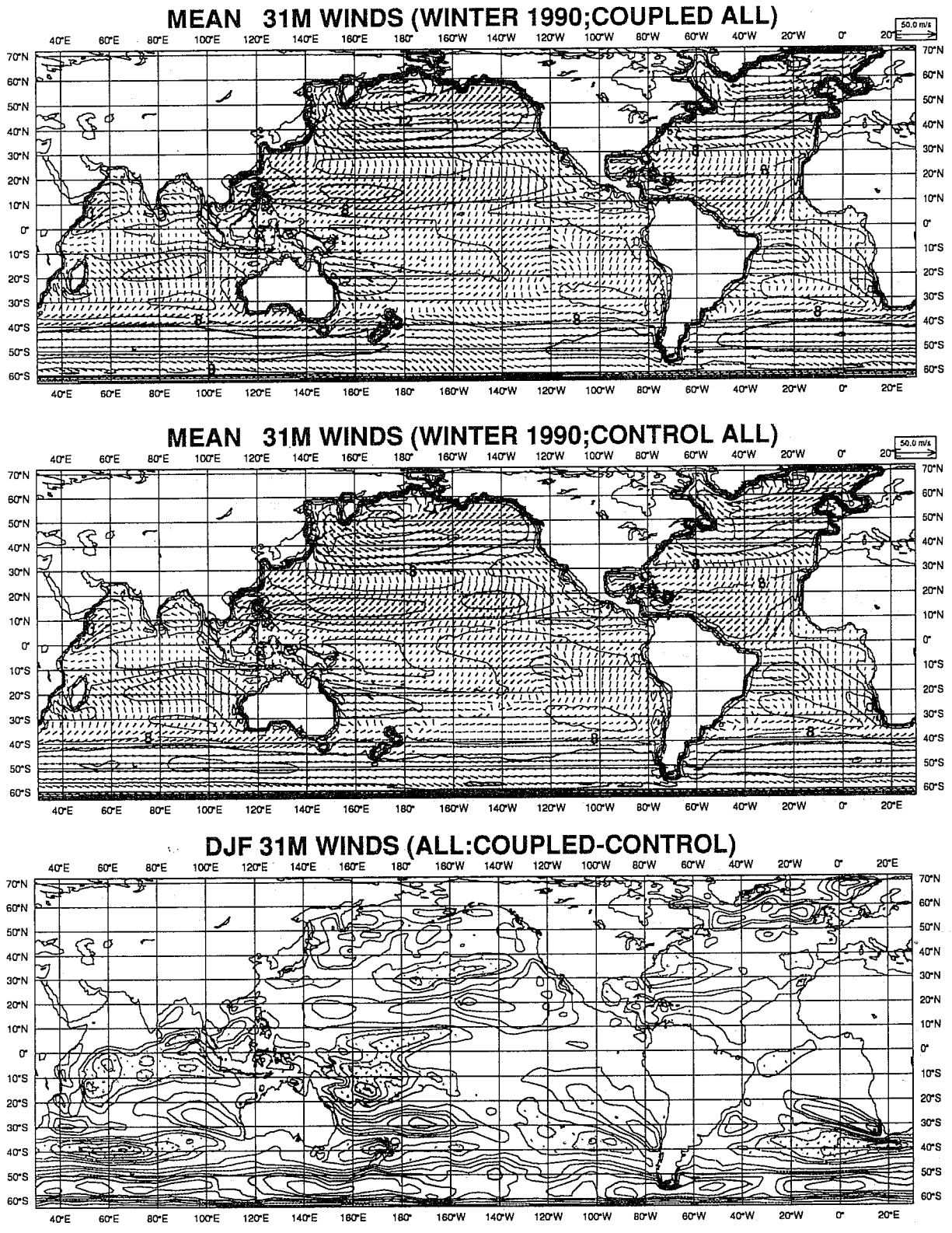

Fig 27 Ensemble mean of 31 m wind for coupled and control run for winter 1990 and the difference.

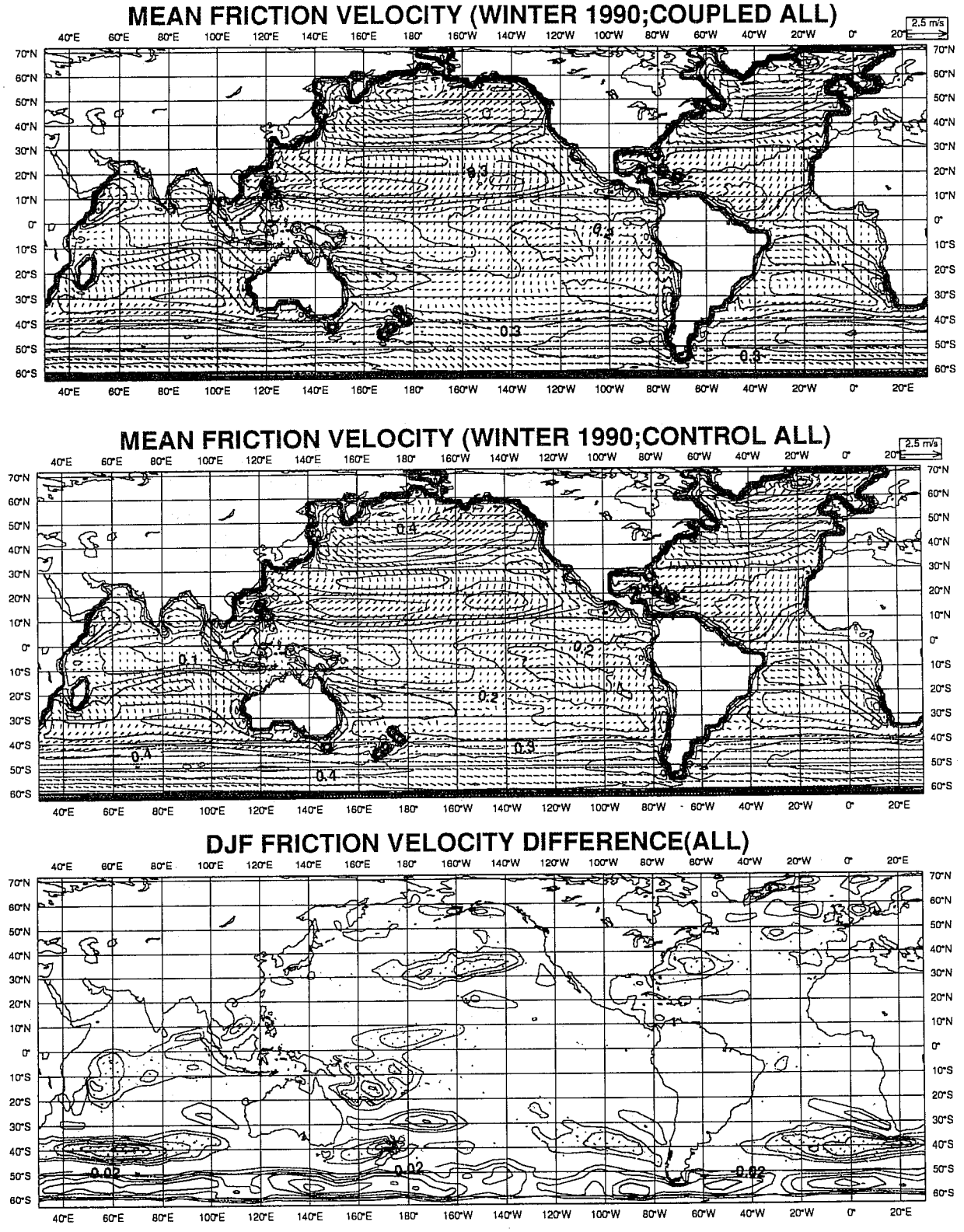

Fig 28 Ensemble mean of surface friction velocity for coupled and control run and the difference.

surface becomes systematically rougher. It is tempting to explain the latter feature by noting that the prevailing wind in that area is north-westerly and therefore the ocean waves are fetch-limited resulting in an increased roughness because the waves are relatively young. We cannot offer such a simple explanation for the other observed differences in surface friction.

It is of interest now to discuss the resulting differences in the atmospheric circulation pattern. In Figs 29 and 30 we have therefore plotted the ensemble mean of 500 and 1000 mb height field and their differences in the Northern and Southern Hemisphere respectively. The symbols used in these plots require some explanation. Contours in the mean plots of 1000 mb height are plotted every 30 m while contours in the 500 mb height field are plotted every 60 m. Contours in the 1000 mb difference fields are given every 10 m while in the 500 mb difference fields they are given every 20 m; in addition, full lines denote positive differences between coupled and control and dashed lines denote negative differences. In the difference plots we have also indicated the results of the t-student test by means of thin lines and shading. Recalling that the t-student test tests the hypothesis whether two fields are identical or not, the light shading denotes the probability of 80% that two fields are not equal while the dark shading denotes a probability of 95%. With this convention in mind we now inspect the difference plots in Figs 29 and 30. Again we observe that the amplitude of the difference between the ensemble means of coupled and control run is much smaller compared to the results of a single run (cf Fig 20). Regarding the Northern Hemisphere we note large differences over the North-East Pacific and the North Atlantic, although they are not statistically significant (probability >70%) because of the large variability of the atmosphere over the oceans. Only the changes over Western Europe and the east coast of North America may be regarded as statistically significant. The impact of the increased roughness over ocean waves on the Southern Hemisphere circulation, on the other hand, may be regarded as considerable. The circulation in the coupled run is clearly less zonal compared to the control run, as is evident east of New Zealand. The correspondence between the difference in friction velocity (Fig 28) and the 1000 mb height difference of Fig 30 is rather evident, although it is not at all clear whether the difference in 1000 mb height fields is caused by the difference in surface friction. But there is no doubt a relation between the two, as is suggested already by Eq (17).

Finally, in Figs 31 and 32 we show the similar results for the geopotential height for the summer runs of 1989. Significant differences may be observed over the southern ocean near the South American continent and south of Australia while moderate differences may also be noted over the North Pacific and North America.

We conclude from this investigation of Monte Carlo forecasting with the coupled WAM-ECMWF model that two-way interaction has a significant impact on the climate of the atmospheric circulation. Anticipating the development of one model for our geophysical system, including a coupled ocean-atmosphere model

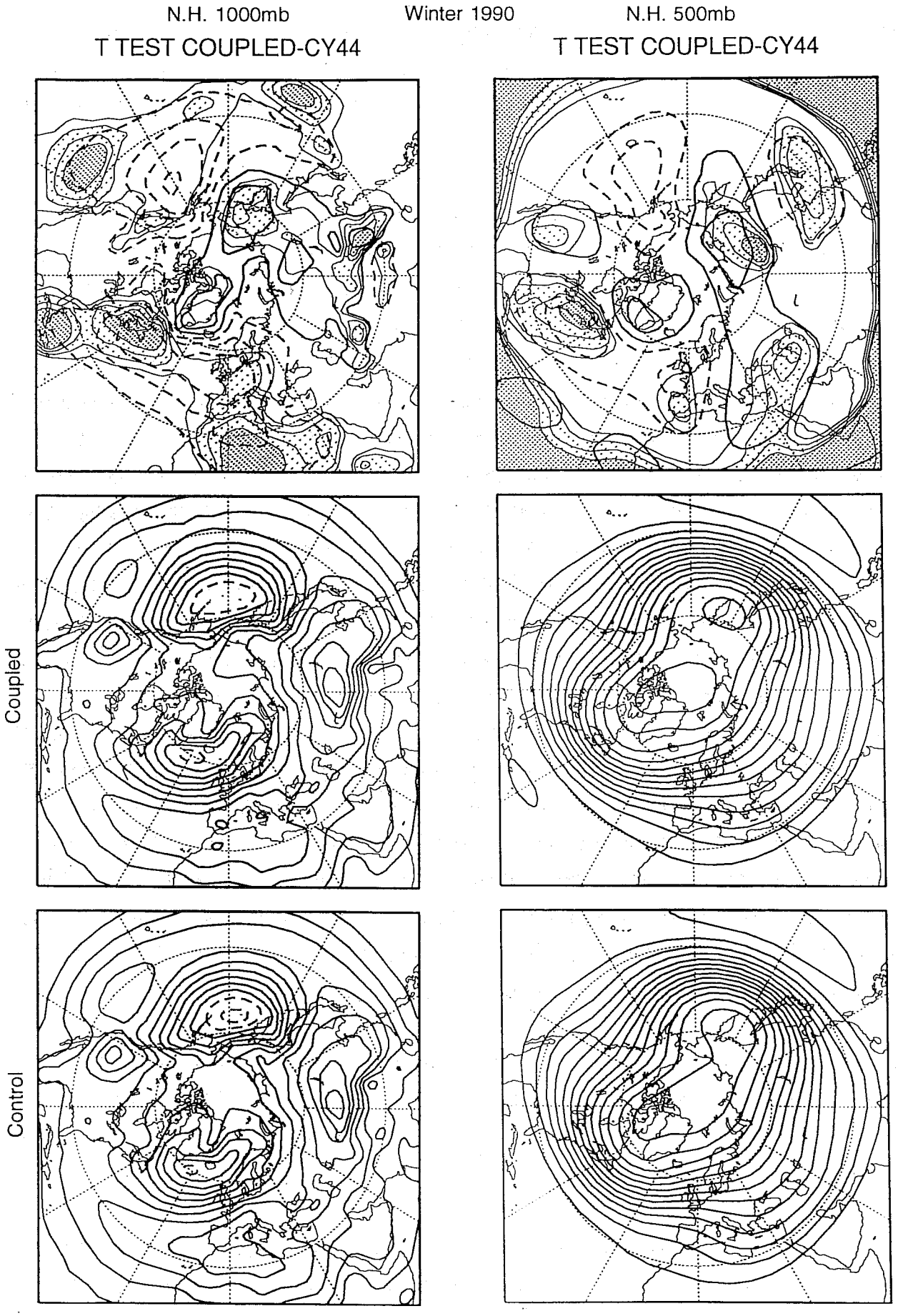

Fig 29 Ensemble mean of 1000 and 500 mb geopotential height of coupled and control run and their differences. Area is Northern Hemisphere and period is Winter 1990.

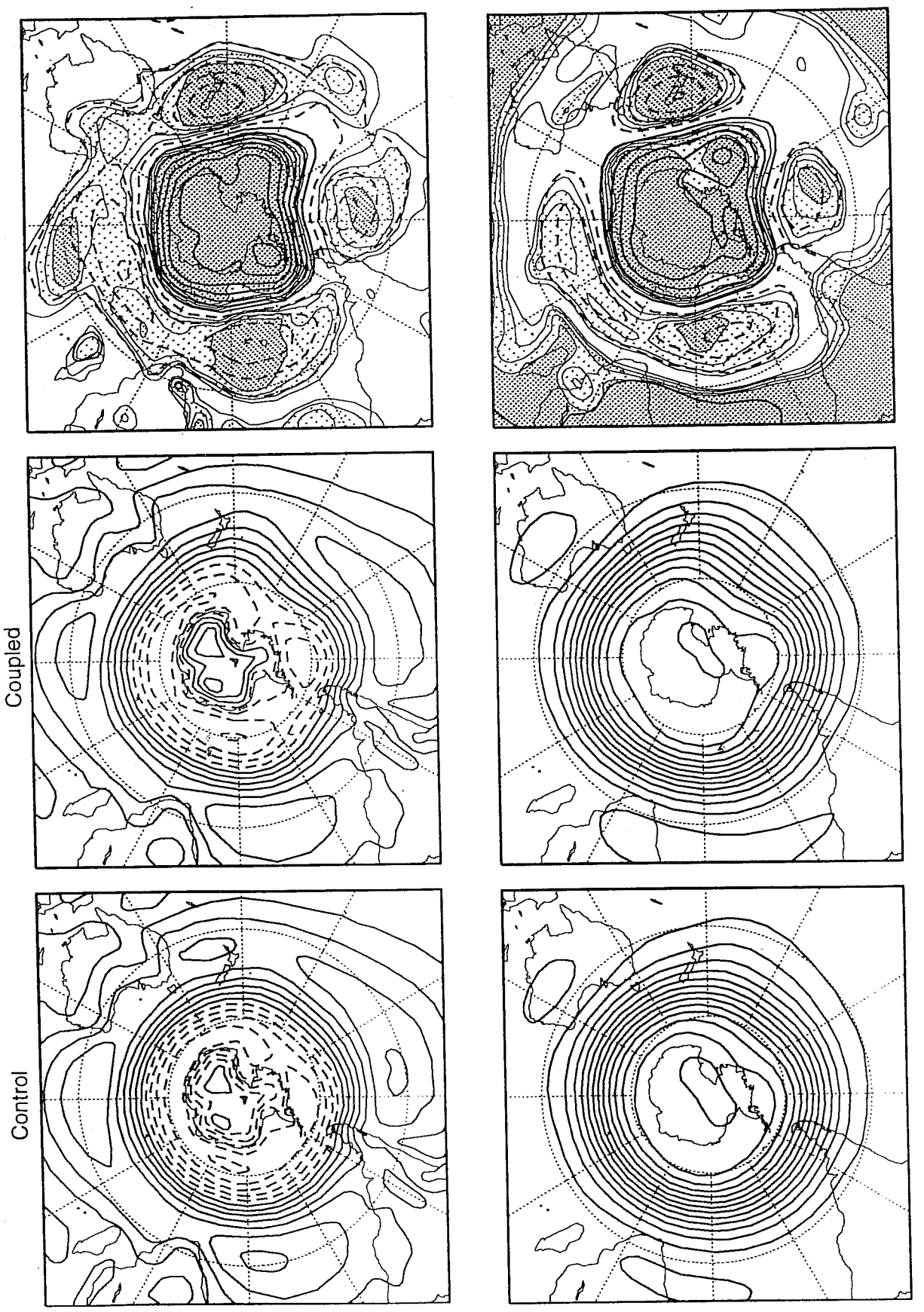

Fig 30 Ensemble mean of 1000 and 500 mb geopotential height of coupled and control run and their differences. Area is Southern Hemisphere and period is Winter 1990.

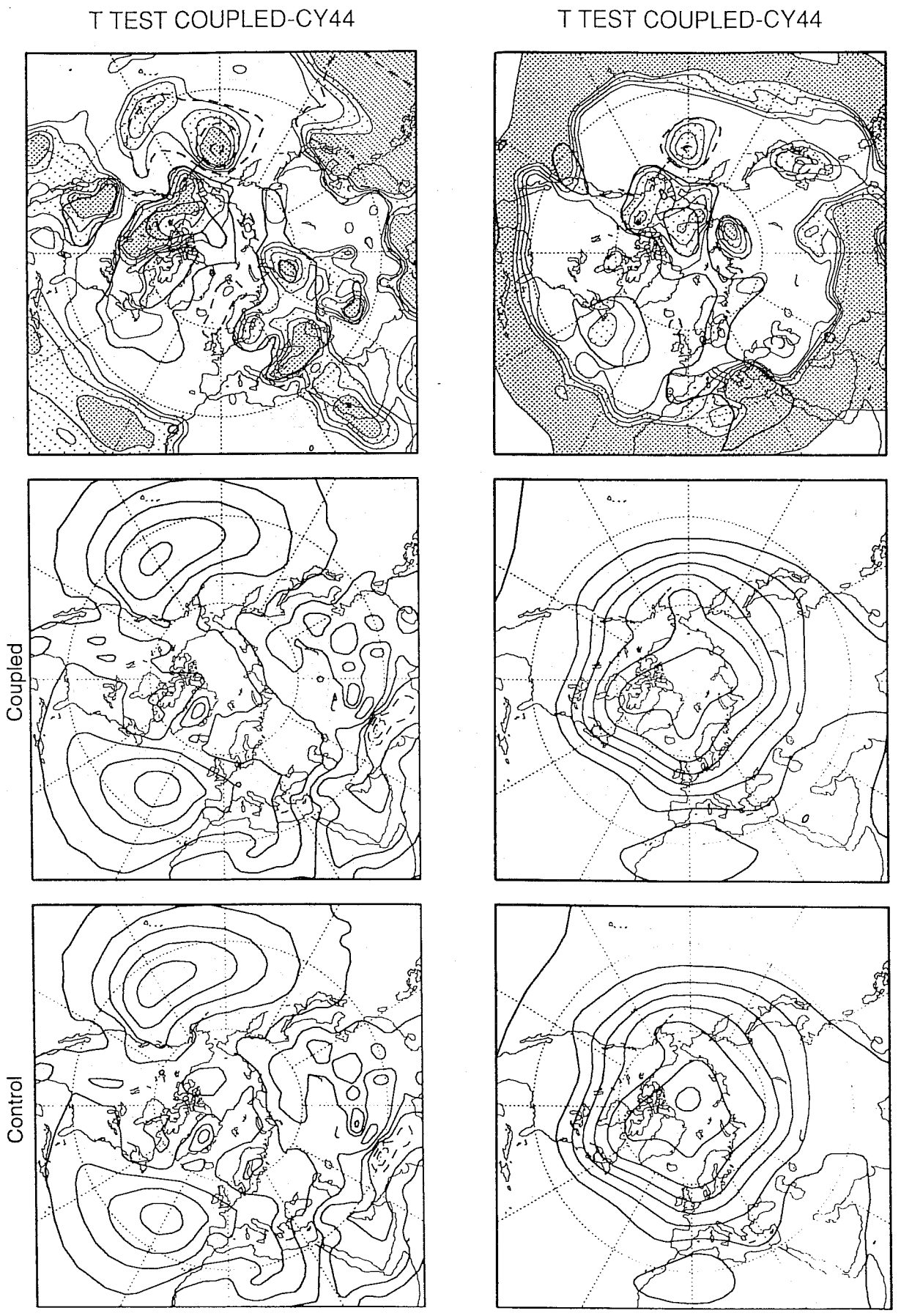

Fig 31 Ensemble mean of 1000 and 500 mb geopotential height of coupled and control run and their differences. Area is Northern Hemisphere and period is Summer 1989.

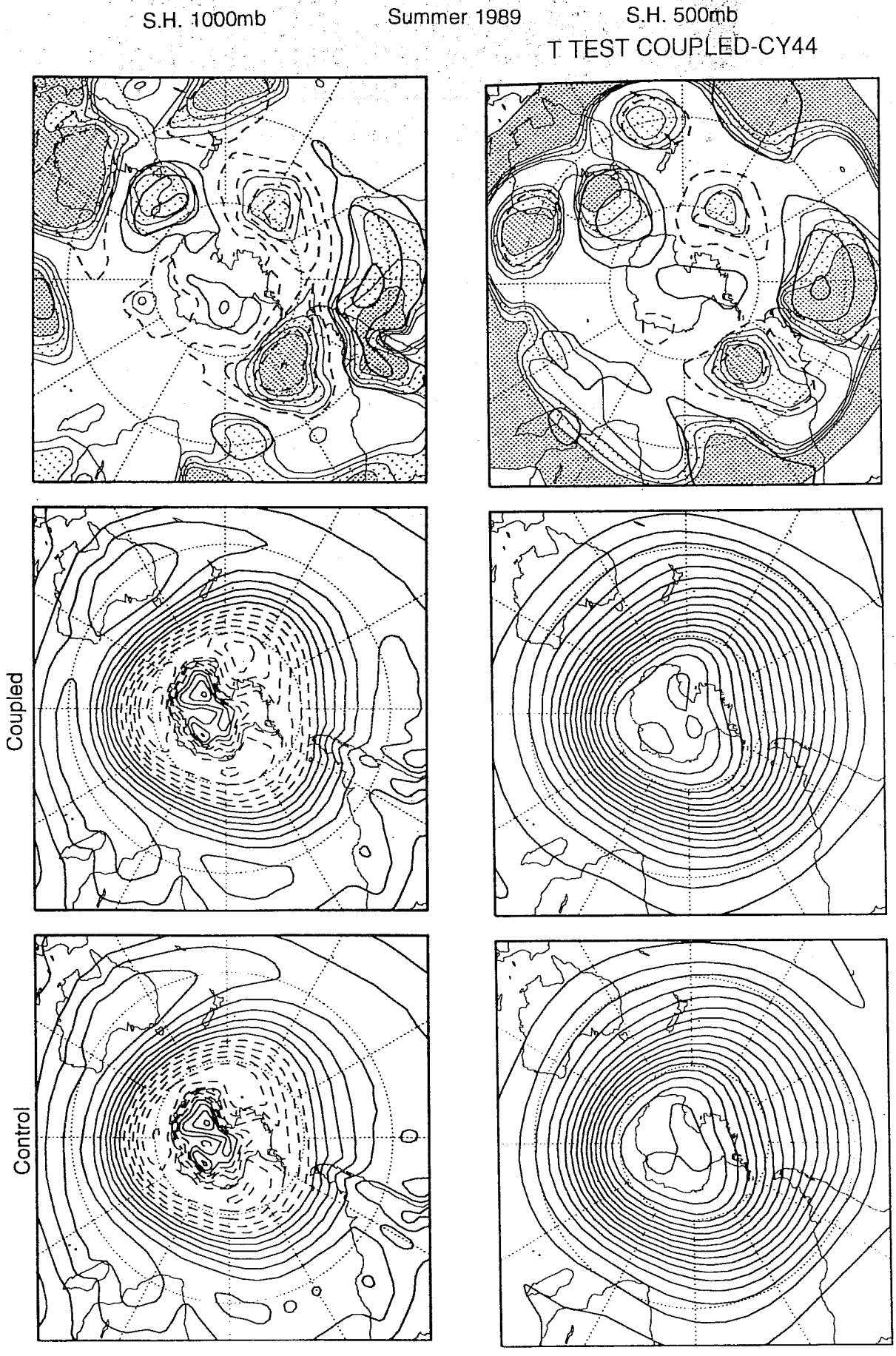

Fig 32 Ensemble mean of 1000 and 500 mb geopotential height of coupled and control run and their differences. Area is Southern Hemisphere and period is Summer 1989.

where the ocean-wave model provides the necessary interface between ocean and atmosphere, the wave-dependent surface stress may induce significant changes in the ocean circulation and therefore in the temperature distribution of the ocean. In its turn, this may affect the climate of the atmosphere as well. As a first step in this direction, Dave Anderson of Oxford University forced an ocean model with the stress fields from the first winter run of 1990. Because only 3 months of surface stress fields were available, abarotropic model which responds to 'high' frequency forcing was used. Results for the mean surface elevation of the ocean surface are displayed in Fig 33. The amplitude of the difference elevation is found to be a significant fraction of the mean elevation of the control run, suggesting that the differences in surface stress are quite large as far as ocean modelling is concerned. Further, there were significant differences in the variance of the surface elevation between the two ocean runs. Since the surface height variability is of several cm amplitude, it is a nontrivial part of the altimeter signal. More work in this direction is needed, however, as obviously one needs to do Monte Carlo forecasting with the ocean circulation model as well, in view of the large differences in the mean stress fields when the initial data are changed. Also, the impact of changes in latent heat flux, which are quite large in the North Pacific (cf Fig 22), are worthwhile to be investigated.

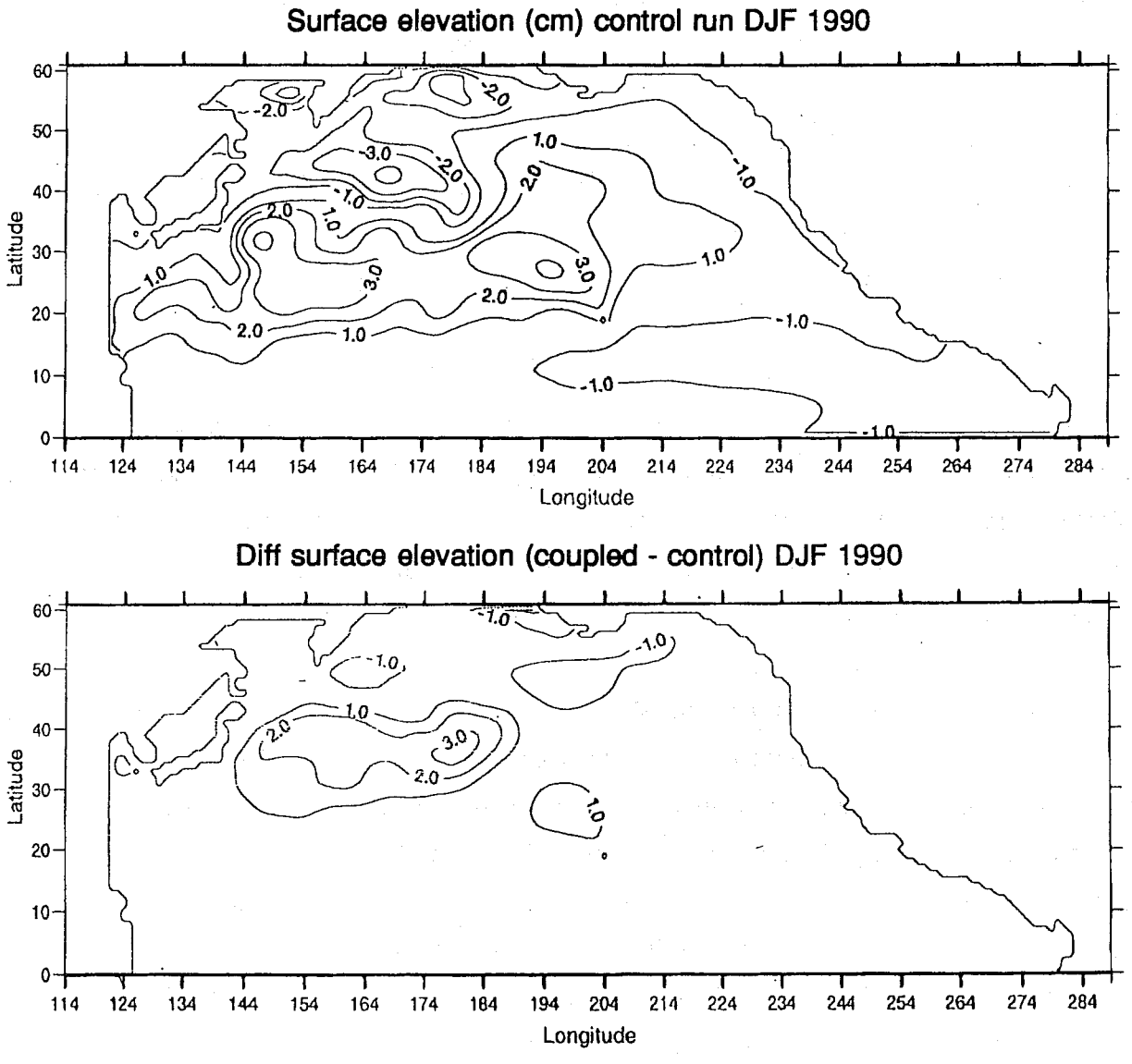

Fig 33 Surface elevation (cm) of barotropic ocean circulation model for control run. Difference between coupled and control is shown as well.

4. SUMMARY OF CONCLUSIONS

This concludes the interim report on the assimilation of wind and wave data to produce global flux fields.

Results presented in this report suggest that it is worthwhile to further develop a coupled ocean-wave, atmosphere model to produce global flux fields. One important reason is that the radar backscatter depends not only on the local wind speed but also, to some extent, on the history of wind field through its dependence on the state of the long waves. Therefore, when assimilating scatterometer data, it seems most natural to do this in the framework of a coupled ocean-wave, atmosphere model.

Another important reason is that the surface friction is found to be dependent on the sea state. This dependence on the sea state resulted in a small, beneficial impact for medium range forecasting while a significant impact on the 90 days mean state of the atmosphere was found. This suggests that a reliable analysis of surface fluxes may only be performed in the context of a coupled ocean-wave, atmosphere model.

Furthermore, it should be realised that, once analysed surface fluxes may be produced in this way, it is important to know whether these fluxes will produce significant changes in the climate of an ocean circulation model. Although the integration period with Dave Anderson's ocean model was only 90 days (so we cannot make claims regarding the ocean climate) we already have strong indications that inclusion of a sea state dependent surface stress will have a definite impact on the climate of the ocean circulation.

Finally, it should be pointed out that the conclusions in this report seem at variance with the ones obtained by *Weber et al* (1993) who concluded that, in state-of-the-art climate general circulation models, wave growth is not a relevant process for the large-scale atmospheric circulation. The conclusion of Weber et al was based on the coupling of a preliminary version of CY4 of the WAM model with the T21 version of the ECHAM model. However, it is well-known that the strength of depressions in such a coarse resolution model is too low. In addition, the time-split integration scheme results in surface stresses which are too weak compared to the surface winds. This reduction of the drag coefficient is especially large in T21 atmospheric models because of the large time step of ½ hour (*Janssen et al*, 1992). The combined effect causes too low wave heights and reduces the impact of the surface stress on the atmospheric circulation. In fact, in this report we have shown that with a T63 version of the atmospheric model the ocean waves have a pronounced effect on the large-scale pressure distribution and therefore on the atmospheric circulation.

Acknowledgement

The support of A Beljaars, J Janssen, P Viterbo, H Wallbrink and P Woiceshyn is gratefully acknowledged. Discussions with L Ferranti, A Hollingsworth and A Simmons are much appreciated. The first part of this research (Chs II-III.3) was supported by BCRS (project 4.1/TO-06), while the second part (Chs III.3-III.4) was supported by the NWO/NOP platform (#853075).

References

Bahar, E, 1981: Scattering cross sections for random rough surfaces: full wave analysis. Radio Science, 16, 331-341.

Chalikov, D V and V K Makin, 1991: Models of the Wave Boundary Layer. Bound Layer Meteor, 56, 83-99.

Charnock, H, 1955: Wind stress on a water surface. Quart J Roy Meteor Soc, 81, 639-640.

Cubasch, U, 1989: A global coupled atmosphere-ocean model. Phil Trans R Soc London, A, 329, 263-273.

Davidson, K L, C E Skupniewicz, D Ross, R G Onstott, J A Johannessen and O Skagseth, 1993: Relationship between wind stress, backscatter and the directional wave spectrum (NORCSEX-88), submitted for publication.

De Cosmo, J, 1991: Air-sea exchange of momentum, heat and water vapor over whitecap sea states, PhD thesis, Univ of Washington, Seattle.

Donelan, M, 1982: The dependence of the aerodynamic drag coefficient on wave parameters. Proc of the First Int Conf on Meteorology and Air-Sea Interactions of the Coastal Zone, The Hague, The Netherlands, Amer Meteor Soc, 381-387.

Ferranti, L, F Molteni, Č Branković and T N Palmer, 1993: Diagnosis of extra-tropical variability in seasonal integrations of the ECMWF model, submitted for publication.

Fung, A K and G W Pan, 1987: A scattering model for perfectly conducting random surfaces, I model development. Int J Remote Sensing, 8, 1579-1593.

Hasselmannn, K, T P Barnett, E Bouws, H Carlson, D E Cartwright, K Enke, J A Ewing, H Gienapp, D E Hasselmann, A Meerburg, P Müller, D J Olbers, K Richter, W Swell and H Walden, 1973: Measurements of wind wave-growth and swell decay during the Joint North Sea Wave Project (JONSWAP). Dtsch Hydrogr Z, Suppl A, 80, (12).

Holliday, D, G St-Cyr and N E Woods, 1986: A radar ocean imaging model for small to moderate incidence angles. Int J Remote Sensing, 7, 1809-1834.

Hollingsworth, A, 1994: Validation and diagnosis of atmospheric models, dynamics of atmosphere and oceans, February 1994 in press.

Janssen, P A E M, 1982: Quasi-linear approximation for the spectrum of wind-generated water waves. J Fluid Mech, 117, 493-506.

Janssen, P A E M, 1989: Wave-induced stress and the drag of airflow over sea waves. J Phys Oceanogr, 19, 745-754.

Janssen, P A E M, P Lionello and L Zambresky, 1989: On the interaction of wind and waves. Phil Trans R Soc London, A329, 289-301.

Janssen, P A E M, 1991: Quasi-linear theory of wind wave generation applied to wave forecasting. J Phys Oceanogr, 21, 1631-1642.

Janssen, P A E M, A C M Beljaars, A Simmons and P Viterbo, 1992: The determination of the surface stress in an Atmospheric Model, Monthly Weather Review, 120, 2977-2985.

Komen, G J, L Cavaleri, M Donelan, K Hasselmann, S Hasselmann, P A E M Janssen, Dynamics and Modelling of Ocean Waves.

Maat, N, C Kraan and W A Oost, 1991: The roughness of wind waves. Bound-Layer Meteor, 54, 89-103.

Maier-Reimer, E, K Hasselmann, D Olbers and J Willebrand, 1982: An ocean circulation model for climate studies. Tech Rep MPI für Meteorologie Hamburg.

Pedlosky, J, 1987: Geophysical Fluid Dyanmics, Springer-Verlag, New York.

Plant, W J, 1990: Bragg Scattering of Electromagnetic Waves from the Air/Sea interface, in Surface Waves and Fluxes, (G J Geernaert and W J Plant (eds)), Volume II, 41-108.

Sausen, R, K Barthels and K Hasselmann, 1988: Coupled ocean-atmosphere models with flux correction. Climate Dyn, 2, 154-163.

Smith, S D, R J Anderson, W A Oost, C Kraan, N Maat, J De Cosmo, K B Katsaros, K Davidson, K Bumke, L Hasse, H M Chadwick, 1992: Sea surface wind stress and drag coefficients: The HEXOS RESULTS, Bound-Layer Meteor, 60, 109-142.

Snoeij, P, E Van Halsema, J Vogelzang, S Waas, S Zecchetto, H Janssen, W Oost, B Jähne and Ch Calkoen. VIERS-1 Final report Phase 3, BCRS report 92-94.

Tennekes, H and J Lumley, 1972: A first course in turbulence, MIT Press, Cambridge.

Valdes, P J and B J Hoskins, 1987: Baroclinic instability of the zonally averaged flow with boundary layer damping, Journal of the Atmospheric Sciences, 45, 1584-1593.

Valenzuela, G R, 1978: Theories for the interaction of electromagnetic and oceanic waves - a review. Bound-Layer Meteor, 13, 612-685.

Weber, S, H von Storch, P Viterbo and L Zambresky, 1993: Coupling an ocean wave model to an atmospheric general circulation model, Climate Dynamics, 9, 63-69.

Woiceshyn, P and P Janssen, 1992: Sensitivity study - scatterometer retrievals with wave age parameter, Workshop Proceedings ERS-1 geophysical validation, Penhors, France (ESA Wpp-36).